Drucksachenkategorie

# Machine Learning methods for EMG-based stroke patient movement analysis

Maren Künemund

DLR

| RMC, Institut für Robotik und Mechatronik | BJ.: 2014 |
|---|---|
| | IB.Nr.: 572-2014-04 |

# MASTERARBEIT

# MACHINE LEARNING METHODS FOR EMG-BASED STROKE PATIENT MOVEMENT ANALYSIS

| Freigabe: | Der Bearbeiter: | Unterschriften |
|---|---|---|
| | Maren Künemund | Maren Künemund |
| | Betreuer: | |
| | Rachel Hornung | |
| | Der Institutsdirektor | |
| | Prof. Alin Albu-Schäffer | |

Dieser Bericht enthält 45 Seiten, 65 Abbildungen und 4 Tabellen

| Ort: Oberpfaffenhofen | Datum: | Bearbeiter: | Zeichen: |
|---|---|---|---|

I assure the single handed composition of this master's thesis only supported by declared resources

Garching, February 24, 2014 _____

## Contents

# Machine Learning methods for EMG-based stroke patient movement analysis


## Abstract

Stroke causes loss of brain functionality leading to restricted muscle activity on the affected body side. This directly impacts the Electromyography (EMG) signal. In order to develop a robotic rehabilitation system for stroke patients, the signal changes have to be analyzed. Hence, the goal of this master's thesis is to identify the latent dimensionality of EMG data and to derive a criterion for the health status of stroke patients. Thus, an experiment has been conducted with seven stroke patients and two reference subjects. Different machine learning methods have been evaluated. At first, dimensionality reduction techniques c.f. PCA, NMF, and Gain Shape k-Means are utilized and evaluated using clustering scores. Those scores show, that reference subjects have higher values, whereas patients have values below a threshold. Applying PCA and NMF synergies have been identified. In order to preserve at least 95% of the information contained, data of patients need more synergies than data of reference subjects. Furthermore, patients' patterns changes considerably on both sides compared to reference subjects'. These results show that synergies are very promising and insightful to evaluate EMG data. Further investigations are necessary to be able to generalize these findings.


## 1. Introduction

Surface Electromyography (sEMG) is a field of research and has been studied for more than 50 years. With the help of sEMG electrodes attached to the skin, it is possible to measure action potentials of motor units non-invasively. They result from a complex process of neuronal activity, leading to contraction of muscle fibers. Since sEMG is easy to use and no in-depth knowledge is required, it is utilized in a broad field of applications and studies.

Its natural interface allows humans to easily control robotic devices or assist them in their activities (Artemiadis & Kyriakopoulos, 2010). It is applicable for diseased people unable to move on their own, too, e.g. Vogel et al. (2013). In case of stroke patients sEMG helps to understand the biological process of stroke. Further, it facilitates an intuitive interface between patient and rehabilitation devices. For example, the success of robotic devices, like ARMin, used for rehabilitation require appropriate and individual control commands for successful therapy.

Stroke causes a rapid loss of brain function due to disturbance in the brain blood supply. Depending on which area is affected the patient may loose the ability to move, formulate or understand speech or to see (on side of the visual field). Further information can be found in Sandercock (2005) and Warlow et al. (2008)

In order to develop an intuitively, adaptable robotic rehabilitation system for stroke patients, it is necessary to understand changes of EMG signals due to the loss of brain functionality and how this correlates to actual movement.

Reaz et al. (2006) gives an overview of different EMG signal analysis methods and why they are useful for EMG analysis. In his diploma thesis Guillemard (2008) covers lots of dimensionality reduction techniques for applications in EMG analysis. Using this general knowledge machine learning methods for an intuitive human machine interface can be formed. Doerschuk et al. (1983) introduces methods to process forearm muscles for the control of a prosthetic device. A newer approach for this task is introduced by Rafiee et al. (2011). Yet, those procedures rely on subjects with relatively normal signals. The task gets more challenging for stroke patients because of the EMG signal changes. Wolf et al. (2005) studies the impact of stroke on EMG signals with the help of kinetic measures. In (Reinkensmeyer et al., 2003) stroke is investigated by means of reaching grasps and modeled with a population vector. Furthermore, synergies are of great interest: Salman (2009) and Cheung et al. (2009) investigate how synergies change due to stroke and how they reflect the health status. Li et al. (2008) further investigates this by analyzing the dependencies of synergies.

The goal of this master thesis is to evaluate machine learning methods for analyzing EMG signals of stroke patients and to compare them with healthy subjects. In this context, questions about how much information is transmitted and how it can be evaluated are discussed. In the end, it should be possible to classify the stroke impact on patients.

## 2. Methods

This section introduces methods for analyzing the EMG signal. This signal consist of $N$ eight dimensional samples. Those eight dimensions, further re-

ferred to as $E$, are muscle activities recorded by electrodes on one side of the subject. The corresponding setup is introduced in section 3.

All samples from these electrodes form the input matrix $X$ with dimensions $N \times E$. The input vector of a specific electrode $e$ with length $N$ is referred to as $x^e$.

### 2.1. Preprocessing

Before analyzing the signal with different methods, it is preprocessed to aquire better results or to fullfill certain criterions. Preprocessing methods are introduced briefly in the following subsection.

**Artefact Filtering** Visual inspection revealed artefacts as shown in figure 1. Due to their strong impact on results, the data has to be filtered.

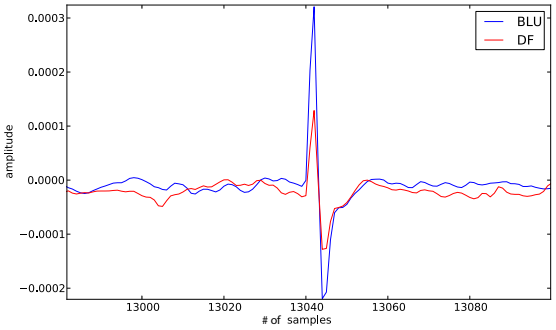


Fig. 1: Example signal (without preprocessing) of an artefact occurring at the exact same sample in different electrodes

These artefacts occur simultaneously in several channels. They have nearly the same shape and are always high in amplitude compared to the rest of the signal. It is therefore straighforward to threshold the signal (in at least 2 channels the threshold has to be exceeded) and then compare it with the help of the pearson correlation coefficient $r_{xy}$:

$$r_{xy} = \frac{\sigma_{af}}{\sigma_a \sigma_f} \tag{1}$$

$$= \frac{\sum_k (a[k] - \mu_a)(f[k] - \mu_f)}{\sqrt{\sum_i (a[i] - \mu_a)^2 \sum_i (f[i] - \mu_f)^2}}, \tag{2}$$

where $a$ is the thresholded signal and $f$ the filter — a signal that has the same shape as an artefact. The filter is visualized in figure 2. If in at least one channel the correlation coefficient is higher than 85%, the detected signal is removed for all channels.

**Centering and Scaling** Lots of machine learning methods require a zero mean and unit variance signal. Therefore, the following shift and scaling is done for each channel seperately:

$$x^e_{cs}[n] = (x^e[n] - \mu^e_x)/\sigma^{e\,2}_x, \tag{3}$$

where $x^e_{cs}$ is the centered and scaled signal, $\mu^e_x$ is the mean and $\sigma^{e\,2}_x$ the variance of the original signal $x^e$.

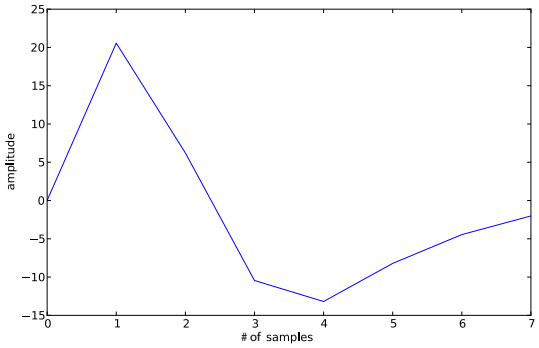


Fig. 2: Filter for pearson correlation coefficient to detect artefacts in signal

The scaling has been adjusted, so that the rest signal (signal with no voluntary muscle activity) has unit variance. Thus, $\sigma^{e\,2}_x$ is calculated by:

$$\sigma^{e\,2}_x = \frac{1}{N} \sum_i^N \left( x^e_{\text{Rest}}[i] - \frac{1}{N} \sum_k^N x^e_{\text{Rest}}[k] \right)^2, \tag{4}$$

where $x^e_{\text{Rest}}$ is a $10s$ signal with no muscle activity.

**Root Mean Square (RMS)** Certain methods require a non-negative signal. An easy method to achieve this is through rectification — using the absolute value of the signal. To simultaneausly smooth the signal, root mean square can be used for each channel $e$:

$$x^e_{\text{RMS}}[n] = \sqrt{\frac{1}{N_w} \sum_{w=0}^{N_w} x^e \left[ n - w + \frac{N_w}{2} \right]}, \tag{5}$$

where $N_w$ is the window size, $n$ is the sample at time $t$ with $n = tT$ and $T$ as sampling interval. With a sampling rate $f$ of 2000 Hz $N_w$ is chosen between 25 ms and 75 ms samples.

**Wavelet Transformation** The wavelet transformation is a time-frequency transformation and is utilized as a preprocessing step to reduce noise. Appendix A.1 gives a brief overview of the definitions of the continuous and discrete transformation.

Here, the discrete wavelet transformation, as defined in equations (A.2) and (A.3), is used for each channel $e$. With the aquired *detailed* and *approximated* coefficients, a soft thresholding is done:

$$C_{\text{thresh}}[n] = \max \left( 0, 1 - \frac{c}{|C[n]|} \right) C[n], \tag{6}$$

where $c = 1$. $c$ is kept fix because the signal has been previously altered by the centering and scaling step. Thereby low energy and unwanted signal during rest periods will be below one and can easily be filtered by thresholding the wavelet coefficients. In the end the filtered noise is aquired by the inverse transformation according to equation (A.4).

The wavelet transformation is build with eight resolution levels and the mother wavelet *Daubechies 6*. The wavelet family is chosen according to the shape of single muscle activation signals and suggestion by Hussain et al. (2008).

### 2.2. Dimensionality Reduction

Section 2 introduced the signal as an $N \times E$ matrix. As $N$ can easily get in the order of $10^4$ and $E$ in areas of eight, it is hard to visualize and unintuitive for humans to understand. Reducing the dimension to two or three allows it to show important relations and helps to improve the understanding.

Reducing the number of dimensions also reduces the computational load. Carefully choosing the number of dimensions noise can also be reduced. This section will introduce several techniques.

**Principal Component Analysis (PCA)** is a linear decomposition method that converts the input matrix into a set of orthogonal and linearly independent vectors — the principal components. These components are the basis vectors that build the transformation matrix $W$. They are stacked as column vectors in sequence of their respective eigenvalues. Using only the first $L$ components with $L < E$ will lead to dimensionality reduction of $X$. The reduced dataset $Y$ can be calculated by

$$Y = XW. \tag{7}$$

The principal components are eigenvectors of the covariance matrix of $X$. Their corresponding eigenvalues are used to describe how much information of $X$ in $Y$ is conserved by using $L$ components. The value in interval $[0, 100]$ is expressed by:

$$\text{info} = \frac{\sum_{\text{l}}^{\text{L}} \lambda_{\text{l}}^2 / \text{N}}{\sum_{\text{i}}^{\Lambda} \lambda_{\text{i}}^2 / \text{N}}, \tag{8}$$

where $\lambda$ is the corresponding eigenvalue. However, in order to independently determine the conserved information and compare it consistently across different methods the reconstruction error is used.

**Non-negative Matrix Factorization (NMF)** is a linear decomposition that approximates $X$ by:

$$X^T \approx WH \tag{9}$$

$WH$ is computed by reducing the squared error

$$E(W, H) = \sum_{k,i} (X_{k,i} - (WH)_{k,i})^2. \tag{10}$$

NMF is purely additive and requires every matrix to be non-negative. It is a sparse representation of $X$ which means that it can encode the data with few components.

To decide how many column vectors for $W$ are needed, the reconstructed signal is compared with the original signal. Analyzing the reconstruction error allows to reasonably decide on the number of components. Further details are explained by Ting & Chvatal (2010).

**Gain Shape k-Means (GSK)** is a derivative of classic k-Means: it tries to find cluster centroids in a dataset, that minimize the distance between data points and the nearest centroid. The number of clusters is defined by $k$. The method can be rewritten as a construcion of a dictionary $D$ with dimension $E \times L$ (where $L = k$). The dictionary $D$ maps $X[n]$ to a output vector $S[n]$. Stacking every output vector for $n = 1 \ldots N$ to one matrix, produces the reduced data matrix $S$ with dimension $L \times N$. Therefore, GSK is not only useful to cluster datasets but to reduce the dimensionality, too.

In order to construct the dictionary, the reconstruction error is minimized by:

$$\min_{D,S} \left( \sum \|DS[n] - X[n]\|_2^2 \right), \tag{11}$$

with

$$\|S[n]\|_0 \leq 1 \forall n \tag{12}$$
$$\|D[l]\|_2 = 1 \forall l \tag{13}$$

as two constraints. Equation (12) with $\|v\|_0$ as l0-norm of vector $v$ states, that at most one non-zero entry is allowed for $S[n]$ so as to keep it simple. According to equation (13) the dictionary $D$ needs to have unit length for every column vector. Otherwise, $D$ can be scaled arbitrarily by describing the same mapping. Constructing $D$ on the basis of equation (11) and the two constraints, distinguishes GSK from the classic approach of k-Means. For further reference see Coates & Ng (2012).

**Evaluation Scores for Dimensionality Reduction** are necessary to make a point about the quality of the reduced space and to compare the introduced methods with each other. I do this by clustering the reduced data with classic k-Means. The obtained labels (with $K$ as the set of clusters) and ground truth labels (with $C$ as the set of classes) are used to evaluate the following scores:

**homogeneity** is defined by conditional entropy $H(C \mid K)$ and $H(C)$ as normalizer:

$$h = \begin{cases} 1 & \text{if } H(C, K) = 0 \\ 1 - H(C \mid K)/H(C) & \text{else} \end{cases} \tag{14}$$

Therefore, $h$ is defined in the interval $[0 \ldots 1]$ where 1 implies each cluster only contains members of a single class (Rosenberg & Hirschberg, 2007).

**completeness** is defined by conditional entropy

$H(K \mid C)$ and $H(K)$ as normalizer:

$$c = \begin{cases} 1 & \text{if } H(C,K) = 0 \\ 1 - H(K \mid C)/H(K) & \text{else} \end{cases} \tag{15}$$

Therefore, $c$ is defined in the interval $[0 \dots 1]$ where 1 means all members of a class are assigned to the same cluster (Rosenberg & Hirschberg, 2007).

**v-measures** harmonic mean of the above: $v = 2\frac{hc}{h+c}$ (Becker, 2011)

**silhouette score** is defined in the interval $[-1 \dots 1]$ by

$$s = \frac{b-a}{\max(a,b)}, \tag{16}$$

with $a$ as the mean distance of points in the same class and $b$ as the mean distance of the nearest class' points, see Rousseeuw (1987).

### 2.3. Synergies

Synergies are components that interact in a system. They produce an effect that can be different or greater than the sum of their individual effects (Corning, 1998).

Muscles of the human body act in a similar way. Different kinds of muscles are activated at the same time to produce a movement. For example, clenching the fist is composed of several muscle contractions in the forearm.

PCA and NMF are methods for data decompositions. They can be used to analyze synergies in EMG signals. Equation (7) introduced PCA as a dimensionality reduction method. To decompose the signal $X$ it must be redefined:

$$X = YW^T \tag{17}$$

Since the principal components are perpendicular, the inverse of matrix $W$ (with all principal components) simplifies to $W^T$ (Golub & Van Loan, 1996). Each of the column vectors of $W$ represents a synergy and each row refers to the corresponding muscle. The value indicates how much this muscle contributes to the signal for that synergy.

The number of required synergies is determined by how much information should be preserved of the original signal. This is done by calculating the reconstruction error as clarified in section 2.2. In this thesis the threshold is set to 95%. That means, with the help of $L$ number of synergies, 95% of the original signal's information must be preserved.

## 3. Experimental Setup

### 3.1. Patients

The experiments have been conducted in Benedictus Hospital in Tutzing (Bavaria), a hospital specialized in stroke patients. Seven patients have been examined, further referenced by their ID `P_N` with $N = 1 \dots 7$. Table 1 gives an overview of their health status and basic parameters at the time of recording. The patients have been chosen so that their stroke impact ranges from slightly to strong. In case they could not move the affected limb on their own, the exercise was recorded twice: once without external aid and once with. This is indicated in column *aid* in table 1. No medical report about their stroke status has been available for this experiment. Therefore, they are classified into groups that rely on observable features. These groups are:

| ID | gender | age | impaired arm | group | aid |
|---|---|---|---|---|---|
| `P_1` | male | 45 | left | D | yes |
| `P_2` | male | 60+ | unknown | B | no |
| `P_3` | female | 60 | right, left 1 year ago | B | no |
| `P_4` | female | 66 | left | D | yes |
| `P_5` | female | 78 | right | C | yes |
| `P_6` | female | 78 | unknown | B | no |
| `P_7` | male | $\approx 80$ | right | D | yes |
| `R_P` | male | 25 | - | A | no |
| `R_R` | female | 25 | - | A | no |

Tab. 1: Overview of patients parameters

A healthy
B no visible impairment in movement
C impairment is visible
D hardly any no movement observable

I excluded `P_1` from the subsequent discussion, since I switched the experimental setup.

For reference two healthy subjects have been recruited. Their IDs are `R_R` and `R_P`. Basic parameters are also included in table 1. They did every excercise twice with some time interval in between to be able to check the consistency of the methods. These repetitions are numbered at the end of the IDs, e.g. `R_R1`.

### 3.2. Excercises

In general there are two kinds of excercises: one that involves movement and one that involves contraction. At the start of each session I have recorded 10 s without any movement or force in order measure the baseline signal. Table 2 gives a description of each excercise.

The movement excercises are chosen such that they only involve one joint. `PA` is an exception to also investigate more complex movement. In general, movements are performed with two degrees, half and maximum amplitude. `AA` was extended to also investigate a different force level. `RF` is a rotation that does not have several amplitudes or force levels. The second group, contraction excercises, investigates the forearm muscles (`CF`) and the overall activation of muscles (`CO`).

Each excercise has been repeated four times within one recording. They are devided into phases: *rest*, *up*,

| ID | Used joint | description | degree |
|---|---|---|---|
| UAF | shoulder | move upper arms forward | 45, 90 |
| UAS | shoulder | move upper arms sideward | 45, 90 |
| AA | elbow | angle arm | 45, 90, weights |
| CF | hand | clench fist | |
| RF | wrist | rotate forearm | |
| CO | no | upper body co-contraction due to putting pressure on table | |
| R | no | resting | |
| PA | shoulder, elbow | moving sheet of paper on the table | |

Tab. 2: Description of excercises

| ID | Name |
|---|---|
| BR | Brachioradialis |
| FCR | Flexor Carpi Radialis |
| BSL | Biceps short head, lower |
| BLU | Biceps long head, upper |
| DF | Deltoid, front |
| DS | Deltoid, side |
| PM | Pectoralis Major |
| TM | Teres Minor/Major |

Tab. 3: Muscle names and abbrevations used

*hold*, *down*. To identify these I also have recorded a trigger. A trigger is provoked when starting the movement, holding and releasing the position or force level and finally when returning to the rest position.

### 3.3. Hardware

I have used Delsys' Trigno Wireless System to record muscle activations. This system consists of 16 electrodes that can transmit EMG with a sampling rate of 2000 Hz. They are not only capable of recording muscle activity but also accelerometer data at 500 Hz sampling frequency (Delsys, 2014). 8 electrodes are placed on each arm, left and right. Their positions and abbreviations are stated in table 3.

To also know the absolute position of each limb, Microsoft's Kinect have been used. It records an RGB+Depth (RGBD) video with 30 Hz sampling rate at a resolution of 640 px × 480 px.

## 4. Results and Discussion

This section will apply the methods introduced in section 2.

### 4.1. Dimensionality Reduction

By reducing the number of dimension of the input dataset $X$ (see subsection 2.2), it is possible to visualize the $N \times 8$ matrix intuitively. For this purpose, the scatter plot is introduced. This plot has several subplots arranged in a matrix of dimension $L \times L$ (currently with $L = 3$). A cell $(i, j)$ plots dimension $i$ against dimension $j$, where $i, j = 1 \dots L$ and $i \neq j$. This plot matrix is symmetric, with the lower half being the flipped and rotated upper half. The diagonal axis is left blank, since this would plot a dimension against itself.

In the following, scatter plots of reference subject `R_R1` and patient `P_7` are shown. Their reduced data is obtained by calculating GSK over all excercises shown in figure 3. The signal was downsampled to 200 Hz and only datapoints during hold phase (see subsection 3.2 for further explanation) are plotted to keep it simple.


Fig. 3: Excercise color codings for the following scatter plots

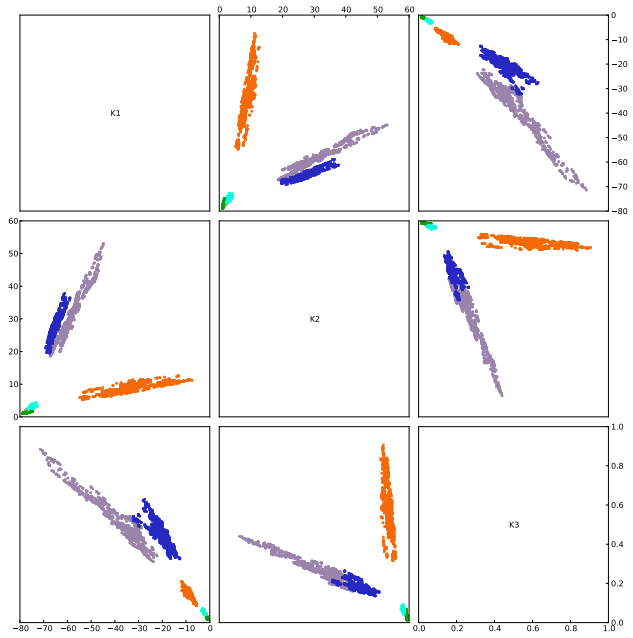


Fig. 4: Scatter plot of reference subject `R_R1`'s left arm dataset. Dimensionality reduction was achieved through GSK. Each point is one sample of an excercise with color label according to figure 3.

Figure 4 shows the scatter plot for reference subject `R_R1`'s left side with visible clusters for excercises `UAF`, `UAS` and `AA`. Points of other excercises reside near the point of origin, indicating a low amplitude of raw data compared to other excercises. Excercise `RF`, e.g., has higher amplitude due to motion and not due to holding the arm in the rotated position.

The scatter plot of group D patient `P_7` (figure 5) contrast with the reference plot. The figure shows the reduced data of the affected side during aided excercises. Only a heap of data points is visible residing in

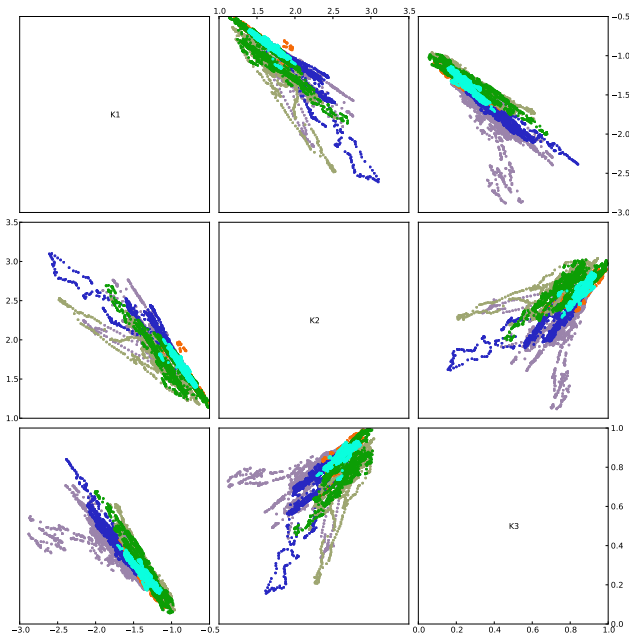


Fig. 5: Scatter plot of patient P_7's right arm dataset (aided). Dimensionality reduction was achieved through GSK. Each point is one sample of an excercise with color label according to figure 3.

| | R_R1 | | P_7 | |
|---|---|---|---|---|
| | left | right | left | right |
| homogeneity | 0.77 | 0.81 | 0.74 | 0.25 |
| completeness | 0.82 | 0.88 | 0.76 | 0.26 |
| v-measures | 0.80 | 0.84 | 0.75 | 0.32 |
| silhouette score | 0.64 | 0.69 | 0.53 | 0.25 |

Tab. 4: Clustering scores comparing reference subject R_R1 and patient P_7 (aided)

a low amplitude intervall. This indicates that all excercises have a low amplitude with nearly no variation making them indistinguishable from each other.

To support the visual impression, the scores from subsection 2.2 are presented in table 4. They are obtained by using k-Means with six clusters. It confirms what was intuitively interpreted. Reference subject R_R1 has higher values (for left and right) indicating a better separability. The affected side of P_7 shows considerably lower values corresponding to the heap of points. The healthy side, however, has values nearly as high as the reference subject. Thus, one can assume that the affected side can be identified by comparing them with the healthy side. The one with distinct lower score seems to be affected by stroke. To verfiy the hypothesis, figure 7 shows scores for every reference subject and patient.

All following illustrations including figure 7 will use the legend displayed in figure 6; with color and hatching code to depict the left or right side and aided and not aided data.

As figure 7 depicts, homogeneity, completeness and v-measures are similar in their values and will be treated as a whole from now on. Furthermore, silhouette

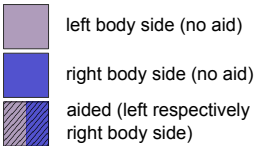


Fig. 6: Legend for illustrations in section 4

scores shows akin trends but with mostly lower values and is therfore not analyzed in detail. In general, reference subjects have higher values than patients. Due to variations, this is not true for all datasets. For example, subject R_P2 has considerably low value. For possible explanation refer to appendix A.4. Patient P_4 has high scores even though she is part of group D. After all, patient P_7 is the only one that has scores compliant to his affected side during both, aided and non-aided excercise.

With the help of those scores, it is also possible to evaluate dimensionality reduction techniques. The introduced methods PCA and NMF can be compared in figure 8 and 9 respectively. In general, all three methods have the same trend: reference subjects have mainly higher values, patient P_4 has nearly as high values as reference subjects and P_7 is the only one, where the values correlate to his affected side consistently. But other than in figure 7, reference subjects have more stable values, scattering around 0.9. That makes it possible to clearly separate reference subjects and patients, with P_4 as the only outlier for PCA and R_P2 for NMF. Summing things up, all three methods are good for visualization. However, due to more stable scores for reference subjects, PCA and NMF seem to find a better representation of the transformation, e.g. by eliminating noise.

The results introduced are useful to show the layout of the data. Since dimensionality reduction projects high dimensional data to a lower space, information can be lost. This can be beneficial for clustering algorithms because the euclidian distance is not appropriate for high dimensions. But in this case, clustering methods in the unreduced space show similar or even better results than in the reduced space (see appendix A.4).

All in all, this subsection has shown the layout of the data in low dimensions and has illustrated which of the applied dimensionality reduction method represents the data in the reduced space best.

### 4.2. Comparism of Synergies in healthy and stroke patient data

This subsection will analyze the synergies of healthy and stroke patient data as introduced in section 2.3 and briefly outline the most remarkable results. For an in-depth analysis refer to appendix A.5.

For a short overview, I refer to excercise CF. It has been selected because it is simple to comprehend which muscles are involved. Normally, only forearm muscles are used. In individual cases the biceps is also contracted

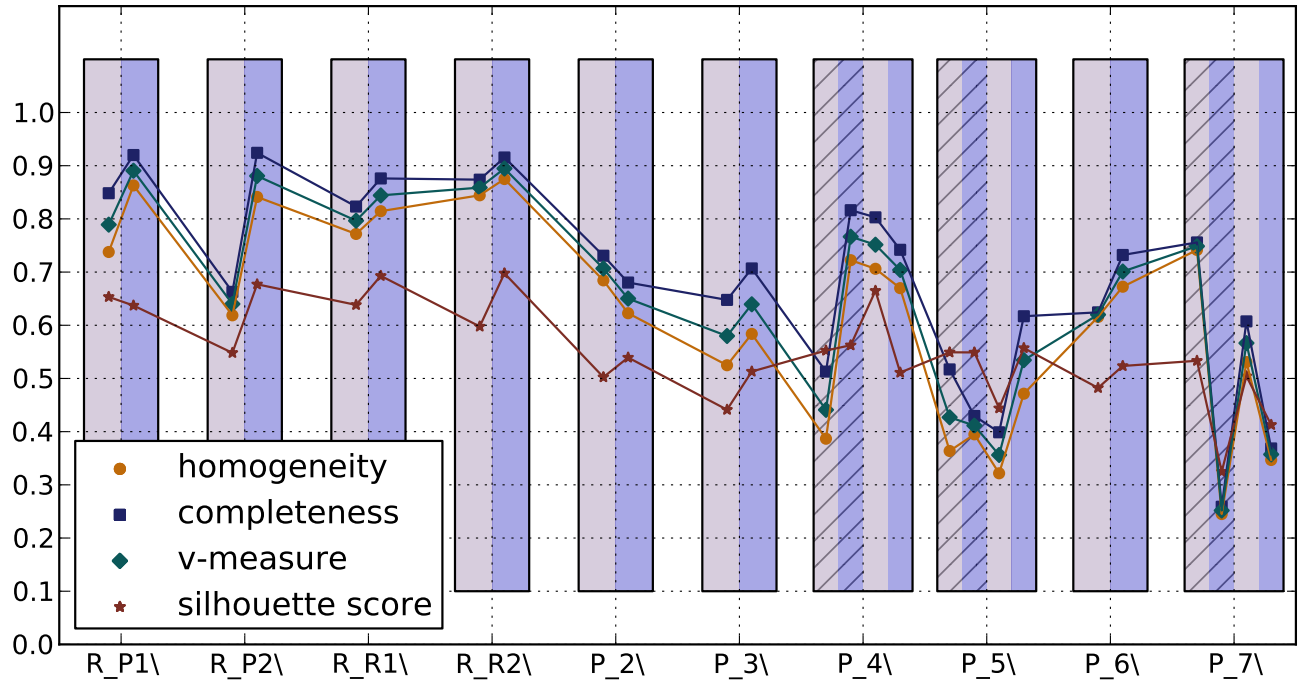


Fig. 7: Clustering scores for each subject. Dataset reduced to three dimensions through GSK and with rectangle color coding according to figure 6.

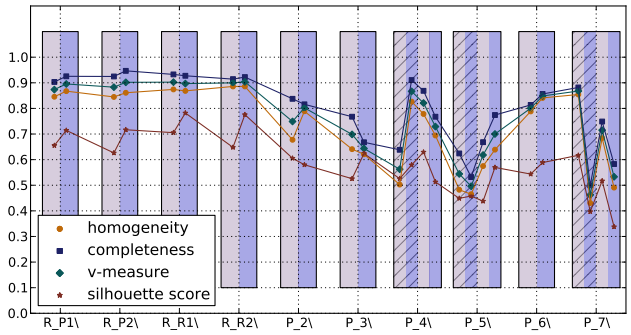


Fig. 8: Clustering scores for each subject. Dataset reduced to three dimensions through PCA and with rectangle color coding according to figure 6.

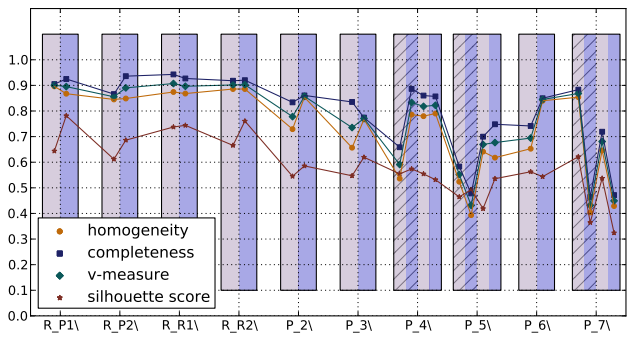


Fig. 9: Clustering scores for each subject. Dataset reduced to three dimensions through NMF and with rectangle color coding according to figure 6.

because some subjects try to increase the force (by cramping their whole arm). In addition, with the help of `CF` most remarkable results can be shown and explained.

A simple way to get a first impression of the data is to count the number of synergies (see 2.3) that are needed to explain 95% of the signal. Figure 10 gives an overview of each subject for excercise `CF`. It shows, that reference subjects do not have more than two synergies. Patients, on the contrary, tend to have more. But as figure 10 shows there are exceptions like patients `P_2` and `P_3`. In this case, the patients are of group B. Their observable impairment is hardly visible and reflects in the low number of synergies. Other exceptions (in different excercises) are discussed in appendix A.5.

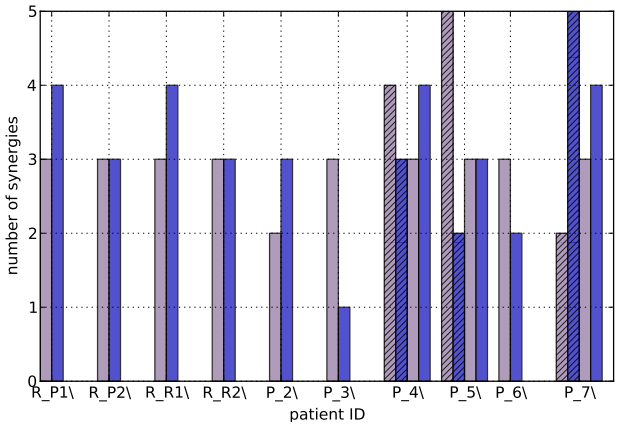


Fig. 10: Number of synergies using NMF for excercise `CF` for each patient and reference subject to reconstruct 95% of original signal, legend see fig. 6

Comparing patient P_2 or P_3 with P_7 shows that patients of group B and D can have the same number of synergies, implying that solely the number of synergies does provide not sufficient information about the impact of stroke. This is even supported within one patient, P_4. She has less synergies on her affected left side (during non aided excercise) than on the right. That is clearly contradictory to the assumption that a stroke leads to more synergies on the affected side.

Therfore, the patterns of synergies are visualized. Since every synergy in NMF positively contributes, they can be summed up to see the overall contribution. This allows to identify which muscles are involved in the movement. The contribution of each muscle is illustrated as a circle and the amount through their size. This visualization is shown in figure 11 for excercise CF. For better comparism circle sizes are normalized for each column.

In general, the patients patterns change compared to thos of the reference group. Even group B's patterns only roughly approximates the healthy pattern. However, in contrast to the other groups, group B's patients tend to have a more symmetric pattern. Nevertheless, there are muscle contributions that are abnormal, e.g. see patients P_2 and P_6. The muscle DF contributes even though it is rarely used by the reference group. This might be because they try to compensate the lack of muscle control in, e.g., the forearm by another muscle group. The abormality is present in both, left and right side.

Group D patients P_4 and P_7 have hardly any visible movement. This is reflected in P_4's left side during aided and P_7 right side during non aided excercise (see figure 11). All circles are approximately evenly sized, implying every muscle contributes uniformly. This can be due to hardly any muscle activation or a very low amplitude of the signal. It can also be an indicator of a low signal to noise ratio (see appendix A.5 for an example).

However, this pattern is seen on patients with a high impairment and can change due to external aid. Even the healthy side is affected (see group C and D patients in figure 11). How this pattern changes can differ. Aiding patient P_4 will lead to a "worse" pattern, the muscle contribution of the affected side is uniform. Aiding patient P_7 the pattern changes slightly, to a more healthy state. Even the healthy side gets more similar to the healthy pattern. Those results can be an indicator of how good the amount of external aid is chosen. In case of P_7 it is appropriate, the signal gets better. But in the other case, the aid seems to be too much, the patient can relax her arm.

To further analyse the impact of external aid on the pattern of synergies, the repetitions within one excercise are visualized in figures 12, 13 and 14. For completeness, patterns of all patients and reference subjects are visualized in figures A.46 to A.45 of the appendix, but are now not explained in detail. Again, the size of a circle represents the contribution of the corresponding muscle. Each column in one rectangle is one repetition of excercise CF. As introduced in 3.2, they are repeated four times ($\pm 1$ due to miscount) in one recording. This visualization allows to see how each muscle's contribution changes within one excercise and to see if the method is consistent under the same conditions.

Reference subjects (their figures can be found in appendix A.7) have a stable pattern. The patterns for patients of group B are relatively stable, too. But, as figure 12 illustrates, variations are possible. Patient P_2 reveals a deviation in the last repetition of the right arm side. This change on one side is also observable on the other side, though not as clearly. Yet, there seems to be a linkage [1] between the left and right side of the arms.

This linkage gets more clear with patient P_4 in figure 13. During the aided excercise her left impaired arm relaxes. As stated before, this can be due to too much aid. Still, her right side has a clearly healthy pattern. However, as no aid is provided (in the other excercise), the muscle contributions of the left arm increase. As though there is some link between both sides, the right side's pattern changes, too — but in a counterintuitive way. This leads to the hypothesis, that synchronous movement causes a symmetric activation pattern. If the left side is involved in the movement, the right side adapts its muscle activation.

Aiding the patient in a likely appropriate manner is shown in figure 14. Patient P_7 has no activity in his right arm during the non-aided excercise. Instead, his healthy arm has a clear activation pattern. Doing the excercise with aid, the healthy pattern changes in a positive way. The affected side's pattern changes, too, but not as significantly due to the paralysis. In the third repetition however, the pattern differs greatly, clearly visible on the healthy side. This can be due to variable external aid (not measured), that has an instant impact on the pattern.

Using only one information like the number of synergies to analyze the data is not sufficient. Interesting results can be revealed and conclusions can be drawn in combination with synergy patterns. It seems even possible to see how much aid is appropriate for the rehabilitation process. However, even though assumptions can be made, these results are based on only six patients and two reference subjects. There are many variations. Thus, a confident generalization is not possible. In the end, the pattern analysis gives a good overview and lets us understand and analyze the effects of stroke better.

[1] This linkage can also be seen on healthy persons. Doing rhythmic excercises with out-of-phase movements of both arms is a hard task and requires alot of practice (see Wiesendanger et al. (1996)).

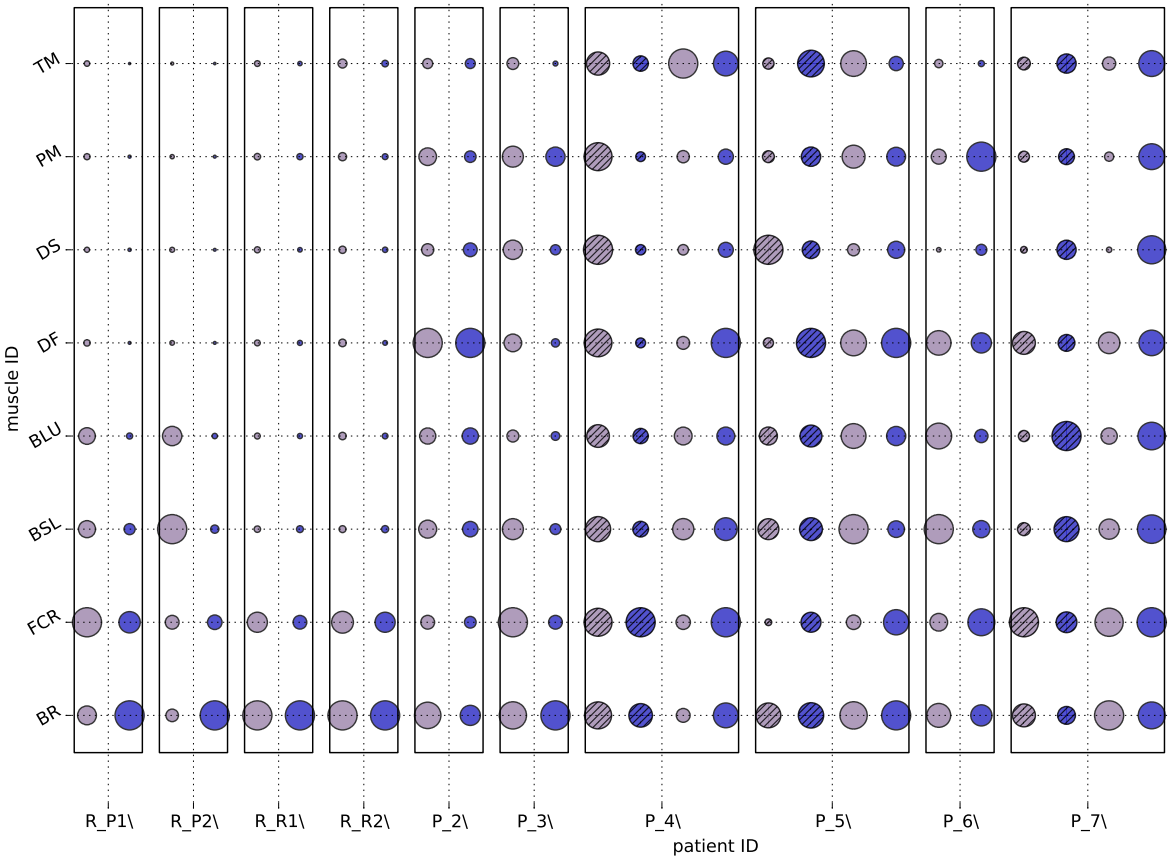


Fig. 11: Muscle contribution for excercise `CF` summed for each synergy and calculated by NMF, legend see fig. 6

## 5. Conclusion

The task for this thesis has been to analyze movement of stroke patients with machine learning methods based on their sEMG signals. In this scope, the following questions have been studied: How does stroke affect the sEMG signal. How much information is contained in the signal? And how big is the intrinsic dimensionality compared to reference subjects?

The analysis has been conducted by means of different methods. First, dimensionality reduction has been used primarily for visualization purposes. It has made obvious that reference subjects have more distinguishable clusters for each excercise than patients. To support this assumption, scores have been calculated comparing the ground truth labels with labels aquired by the clustering algorithm k-Means. It is apparent, that reference subjects have higher scores ($\approx 0.7 \ldots 0.9$) than patients ($\leq 0.7$). Higher scores correspond to correct labeling through the clustering algorithm. That means, lower values arouse due to worse seperability of patients data. Those scores also illustrate that PCA and NMF perform better than GSK. But all in all, they represent the eight dimensional data very well in three dimensional space.

The most promising method is the analysis of synergies. The number of synergies needed to preserve 95% of information is increased for stroke patients. Furthermore, their pattern changes considerably, not only on the affected side but also on the healthy. How this pattern changes and how similar it remains to a healthy could be an indicator for the health status. However, the recorded data is not representative enough to generalize these assumption. A further interesting finding has been, that the pattern also changes due to appropriate or inapproriate aid. Due to too much help, the patient can relax, leading to visible change in the patterns of synergies.

Finally, wavelet energy has also been investigated. Yet, this method turns out to be infavorable. There are no consistent results in relation to stroke patients and reference subjects, let alone the health status of stroke patients.

Further work should pursue promising methods like synergies with NMF. This can be done by comparing healthy patterns with stroke patient patterns and deriving a similarity score that can possibly correlate to the health status of a patient. An automatic pattern analyzation can be implemented in order to see how much aid is appropriate.

Furthermore, other machine learning methods like recurrent neural networks can be used to compare both sides of a stroke patient and see how they differ, e.g. with the help of Kullback–Leibler divergence (Kullback & Leibler, 1951). This can be done by comparing stroke patients with healthy subjects, too.

In order to get even better results, other preprocessing steps than RMS might be needed. RMS has the dis-

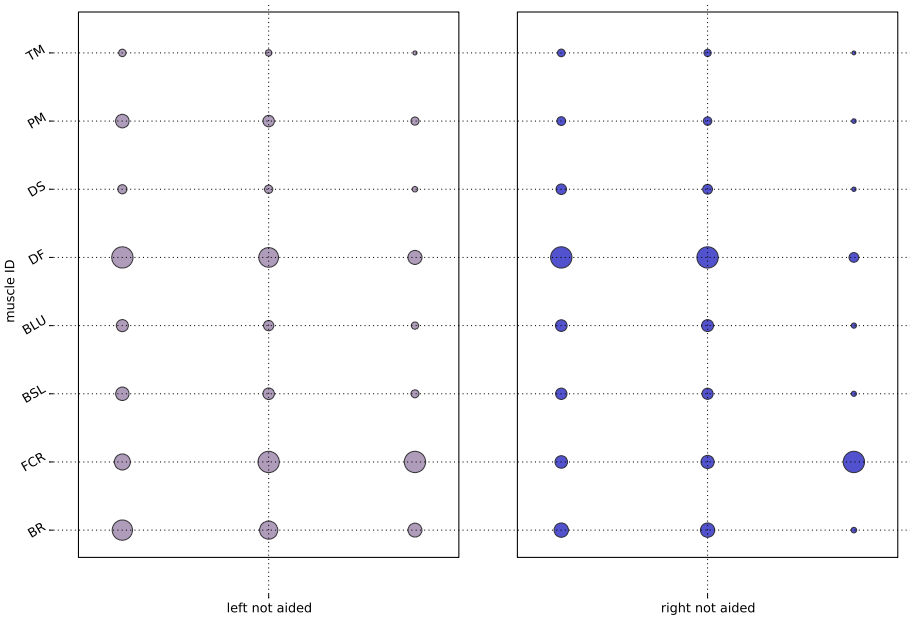


Fig. 12: Muscle contribution summed for each synergy and calculated by NMF for every repetition during excercise `CF` of patient `P_2`, legend see fig. 6

advantage that it is averaging over time. Information about frequency, sign or the signal shape is lost. Yet, this can be overcome with other methods, e.g., windowing samples ($n$ consecutive samples form a new sample).

All in all, this master's thesis has shown promising results. On this basis, further studies can be conducted, and with the help of a higher number of patients and reference subjects, the results can be confirmed and generalized.

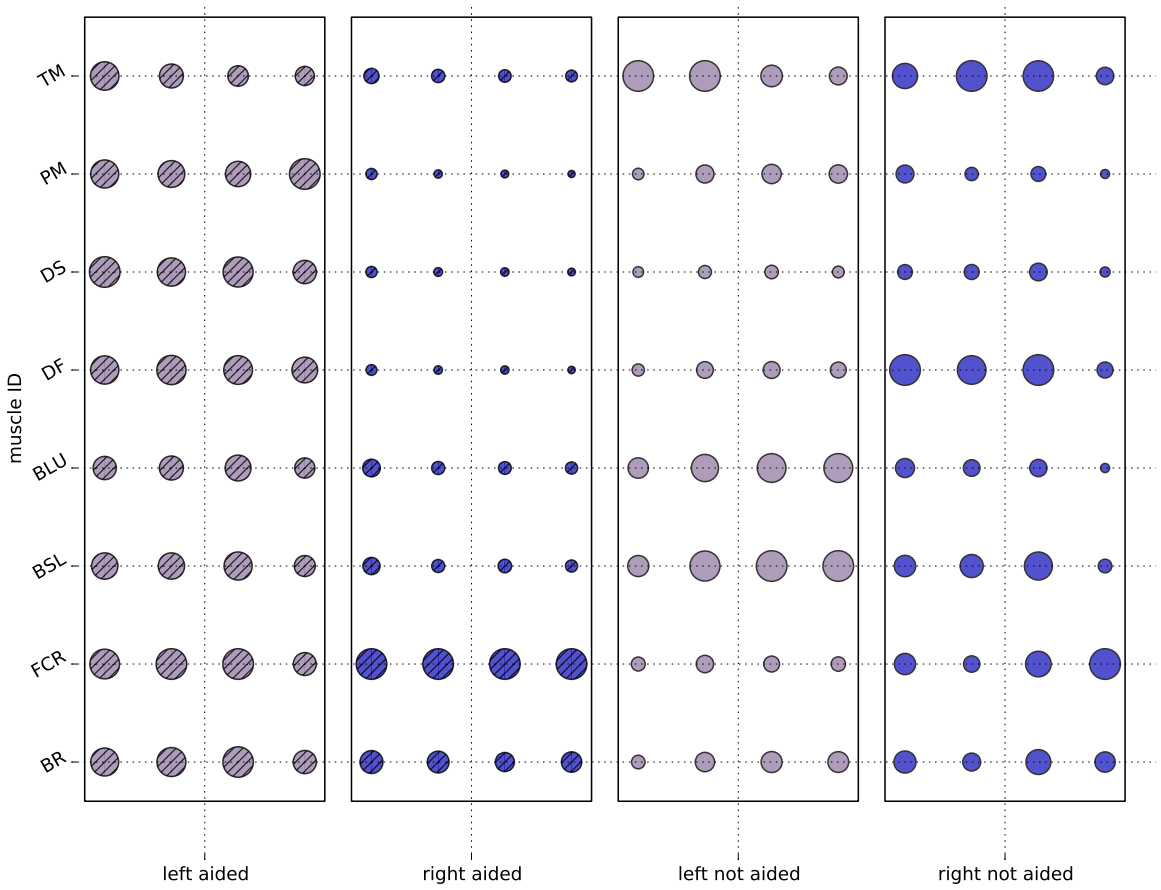


Fig. 13: Muscle contribution summed for each synergy and calculated by NMF for every repetition during excercise CF of patient P_4, legend see fig. 6

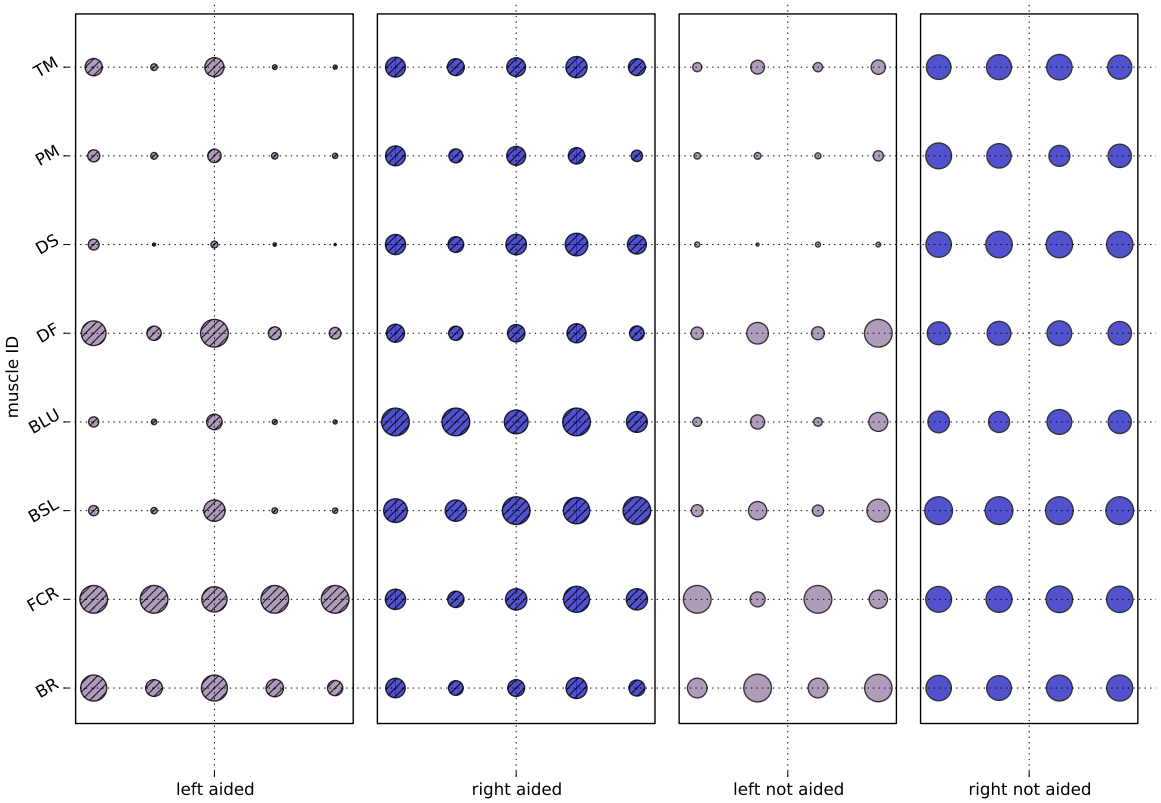


Fig. 14: Muscle contribution summed for each synergy and calculated by NMF for every repetition during excercise CF of patient P_7, legend see fig. 6

# A. Appendix

## A.1. Wavelet Transformation

The continuous wavelet transformation is defined by the following equation:

$$\Psi_x^{\psi}[\tau, s] = \frac{1}{\sqrt{|s|}} \int x[t]\psi^* \left[\frac{t-\tau}{s}\right] dt, \qquad \text{(A.1)}$$

where $\tau$ is the translational shift of the wavelet function in order to move it across function $x$. $s$ scales function $x$, that is looking at the function with different resolution levels. It is antiproportionally connected to the frequency. $\psi$ is the mother wavelet function. In the scope of this thesis the mother function is part of the family *Daubechies* visualized in figure A.1.

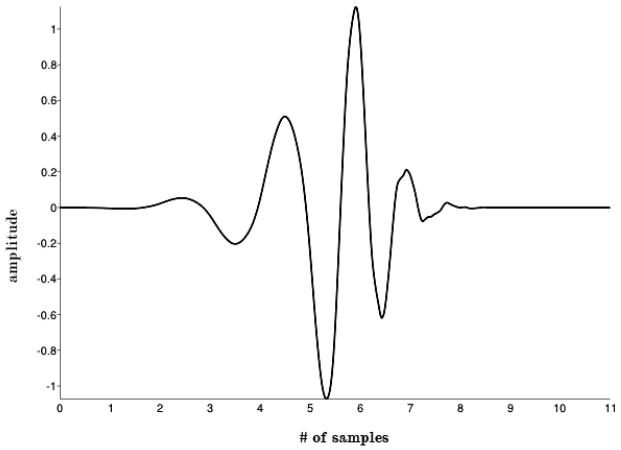


Fig. A.1: Mother wavelet function of family *Daubechies*

In most applications, the discrete wavelet transformation is used. It is obtained by sequentially decomposing $x$ by means of high and low pass filters. The high pass filter $g$ is the wavelet function and will give the so called detail coefficients. The low pass filter $h$ is the scaling function. It will give the approximate coefficients. The following equations will show the decomposition of $x$ for one resolution level.

$$y_{\text{high}}[k] = \sum_N x[n] \cdot g[2k-n] \qquad \text{(A.2)}$$

$$y_{\text{low}}[k] = \sum_N x[n] \cdot h[2k-n] \qquad \text{(A.3)}$$

To obtain a multiresolution wavelet transformation, $y_{\text{low}}$ is further decomposed with each level producing detail coefficients. Finally, the last level of resolution gives the approximate coefficients. The inverse transformation is stated by

$$x[n] = \sum_{k=-\infty}^{\infty} (y_{\text{high}}[k] \cdot g[2k-n]) + (y_{\text{low}}[k] \cdot h[2k-n]). \qquad \text{(A.4)}$$

## A.2. Wavelet Energy

Wavelet transformation is not only used for preprocessing (see 2.1) but also to evaluate the energy of the signal. This is done by using the sum of the absolute wavelet transformation coefficients. The sum is calculated over phases of the signal. For this thesis the definition of a phase is introduced in section 3.2. Each phase has an energy level. Those levels are compared per channel with the left and right arm by using the following normalized difference:

$$\Delta E = (E_{\text{left}} - E_{\text{right}})/(E_{\text{left}} + E_{\text{right}})/2, \qquad \text{(A.5)}$$

where $E_{\text{left}}$ and $E_{\text{right}}$ are the energy levels of the right respectively left side. The method was introduced by Jiang et al. (2013).

## A.3. Evaluation of Wavelet Energy

Wavelet energy was introduced in section A.2 and compares the energy level of the right and left side. A low sum of energy implies that both sides contribute energy evenly. The assumption is, that this is true for reference subjects. A small divergence is possible due to the dominant side. Patients, on the contrary, are assumed to have a clear preference of wavelet energy on one side.

To validate this hypothesis, figure A.2 shows the results of this method. To get *sum*, the energy of every frequence band is added, *low* is built by adding only the first six and *high* by the last six. Considering only *sum*, figure A.2 shows reference subject `R_P` with relatively high values for the left side. In contrast to that, reference subject `R_R` has a very low — even zero — value. Most of the patients have high values on the right side regardless of the affected side. In order to evaluate different frequency bands, low frequencies (coefficients of levels below six) and high frequencies (coefficients of levels above six) are also plotted. For most subjects, they contribute for the same side. But a conclusion about which frequency bands have more impact cannot be generalized.

All in all, there is no correlation that would make a conclusion about the patient's health status reasonable. Even the reference data lacks consistency. Reference subject `R_P` has higher values than some of the patients. Since he is right handed, his high values cannot be explained with his dominant hand. To confirm the discrepancy, the wavelet energy is analyzed for every excercise seperately. This is visualized for all reference subjects in figure A.3.

Although only reference subjects are depicted, it conveys, that there is no correlation to their health status — not only across subjects but also across excercises. No reference subject has consistently low values across several excercises. The side with more energy even changes arbitrarily. On this basis, the assumption that reference subjects have low energy and only on their dominant side is disproved. It turns out, that

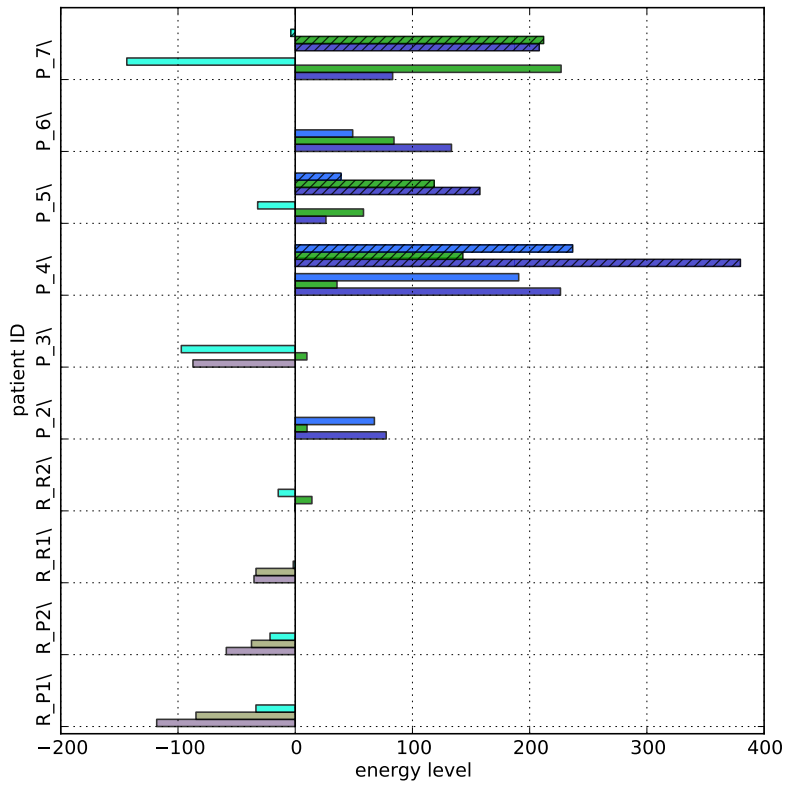


Fig. A.2: Wavelet Energy for each patient summed over excercises listed in figure 3. Values below zeros imply, there is more energy on the left side, positive implies more on the right side.

wavelet energy is not suited to identify the impact of stroke and derive further conclusions.

### A.4. Continued Results for Dimensionality Reduction

This subsections aims to deepen the analysis started in subsection 4.1. The evaluation will concentrate on reference subject `R_R` and patient `P_7`. Other subjects are left out because they show similar results corresponding to their health status.

At first, scatter plots of patient `P_7` (figures A.12 and A.13 in appendix A.7) are investigated. Plots for the aided excercises and left side show visually seperable clusters. The impression is supported by high values for clustering scores (see subsection 2.2) about 0.7 or higher (see figures 7, 8 and 9). On the contrary, the right side shows a heap of points leading to low scores around 0.3. The methods PCA and NMF show slightly higher values because points are more scattered and less dense than those obtained by GSK.

As scores and figure A.13 for `P_7`'s left side already revealed the reduced data is less seperable during the non-aided excercises. Instead, for the same data but on the right side clusters become more distinguishable. Excercises `UAF` and `UAS` even seem to form a new cluster. This insight correlates to the higher score of about 0.5. However, the new layout of datapoints in the reduced space is different for the aided and non-aided excercises.

Reference subject `R_R` shows very good clustering results for both recorded sessions. Opposing to patient `P_7`, the results show similar cluster layouts for the left and right side, as well as for the first and second data recording. Even though there is no perfect match and clusters can be laid out rotated or flipped, their relations to each other are simliar. More dense cluster are formed by `CF`, `RF` and `CO`, whereas `UAF`, `UAS` and `AA` are more sparse.

Figure A.15 depicts another feature of the data. Excercises `UAS` and `UAF` each form not only one, but two clusters. This can be due to different force or lifting levels. These clusters are visible on the left side for all three methods. Yet, consulting the results by using synergies does not reveal abnormalities for this dataset. In order to verify the assumption regarding lifting levels the accelerometer data could be of help.

By inspecting these results, it seems like clustering scores in association with dimensionality reduction are sufficient for classification of healthy subjects and stroke patients. However, figure A.4 reveals, that dimensionality reduction is not necessary in order to obtain akin scores. As already stated in subsection

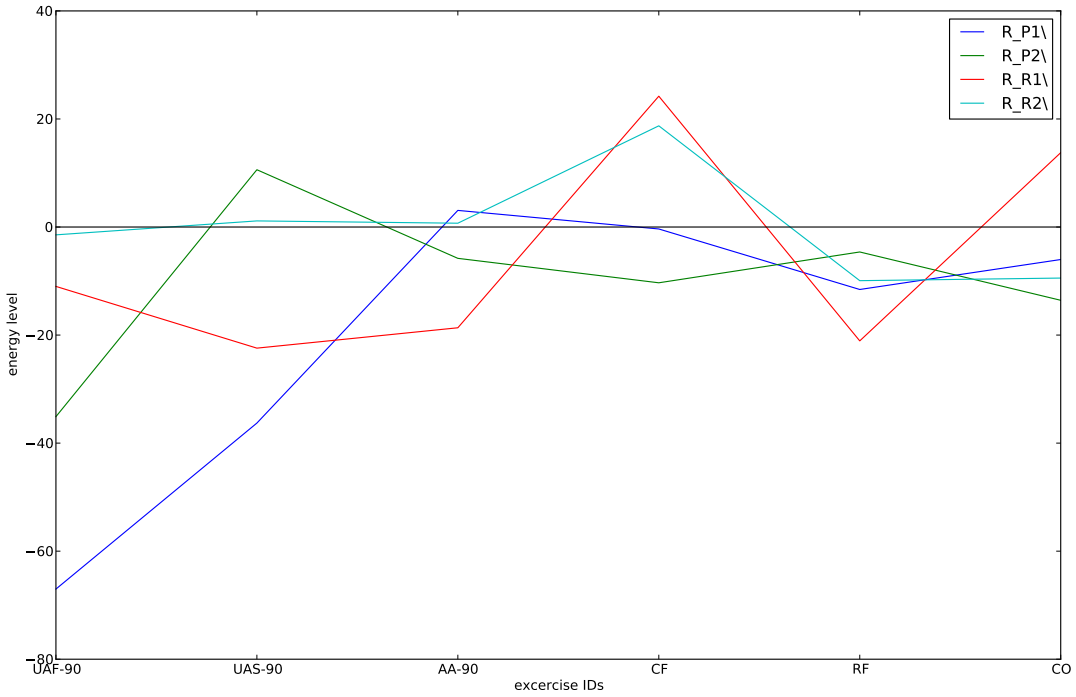


Fig. A.3: Wavelet energy for each reference subject and several excercises

4.1, reference subjects can be distinguished by scores for completeness above 0.9. Yet, clustering scores for unreduced data indicates the same results. This can be due to the fact, that by means of dimensionality reduction information is lost. And reducing the space from eight to three with six different excercises could imply worse clustering scores. However, having quite similar results leads to the following assumption:

- the dimensionality reduction methods are good for this kind of data
- the data spreads only few latent dimensions despite their different excercises
- the preprocessing method RMS neglects most information

The last one is especially feasible because averaging over time will lead to loss of information about frequency, sign and shape of the signal.

Nevertheless, dimensionality reduction could prove useful for evaluating clustering scores when the number of electrodes are higher. Since many methods like k-Means depend on the euclidean distance. And their results can become wrong in high dimensional space. In that case, dimensionality reduction or window samples are inevitable for a proper evaluation.

## A.5. Continued Analysis of Synergies

### A.5.1. Signal Decomposition

On the basis of figures A.16 to A.21 synergy decomposition can be explained and visualized. One figure contains plots for patient `P_7` aided and non-aided and reference subject `R_R2` (top to bottom). Each of those plots consist of further subplots, with the top subplots being a column of the matrix $Y$ (see subsection 2.3), further referred to as synergy contribution, weighted by the corresponding synergy value — the matrix entry of $W$ at the row corresponding to the muscle and column corresponding to the synergy. That means, in order to reconstruct the signal, the same components are used for every muscle but weighted differently. Summing these contributions up builds the reconstructed signal in the bottom subplot in green.

Synergy contributions are signals most akin to signals that have high amplitude and distinctive shape compared to other signals of the input matrix. The contributions try to represent those in order to minimize the reconstruction error. As figure A.16 for reference subject `R_R2` depicts, the strongest amplitude is during the hold phase in the forearm muscles. The synergy contributions are formed by using their shape because they explain most variance. Since only one synergy prevails, forearm muscles `BR` and `FCR` activate in a very similar manner. On the other hand, if the signals are mostly white noise (no distinctive features), more synergies are needed for the approximation. This can be seen in the plot for patient `P_7`, right side, non-aided,

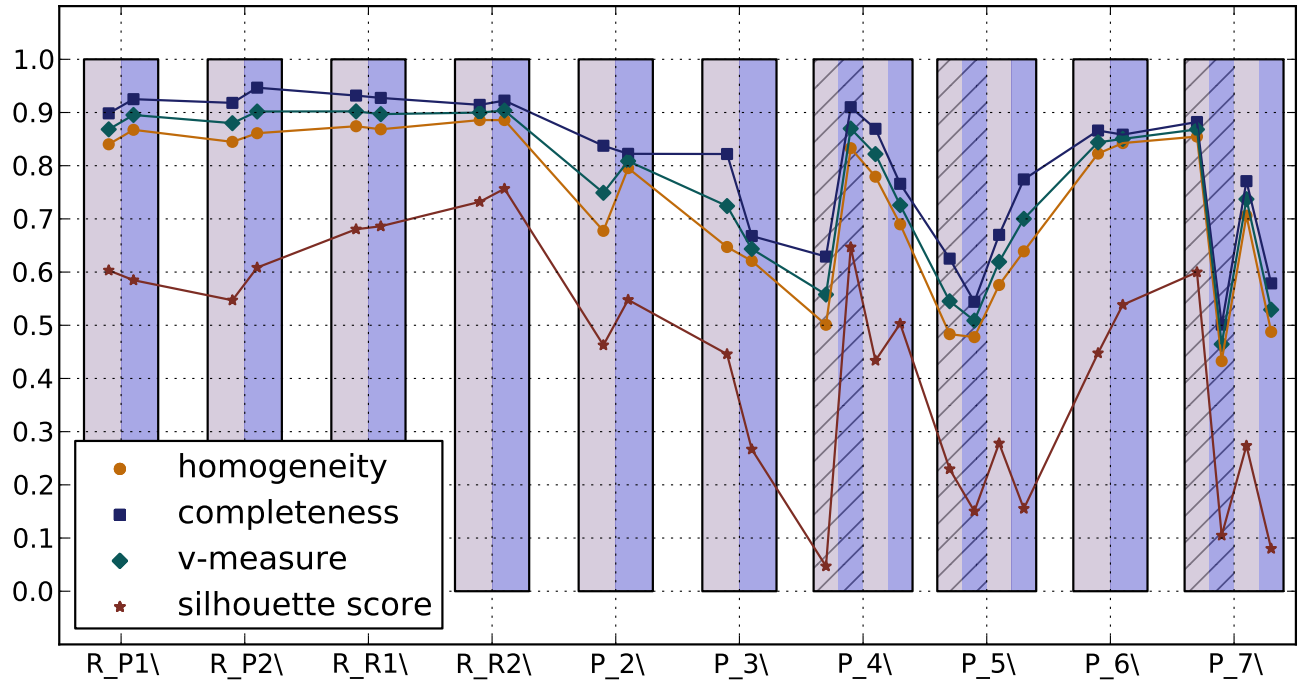


Fig. A.4: Clustering scores for each subject. Unreduced datasets and with rectangle color coding according to figure 6

e.g. figure A.16 and A.17.

In general, inspecting the synergy contributions can reveal the kind of signal that is incorporated in the original signal. It can affect each muscle more or less expressed by a high or low synergy value. Even though the reconstructed signal seems to badly approximates the original (see figures A.20 and A.21), it has no big impact on the reconstruction error, because the amplitude very low (compare y-axis of these plots). Comparing synergy contributions of reference subjects with stroke patients shows that patients have different compositions. They are less intuitively interpretable because the signal resembles noise.

### A.5.2. Analysis of Synergy Values

Subsection 4.2 already discussed the results obtained by NMF. This subsection will also present those obtained by PCA. In contrast to NMF, PCA can also produce synergies with negative shares (compare figures A.22 and A.23 with the top plots for patient P_7 and bottom for reference subject R_R1). Analyzing synergies for excercise CF in figure A.22 shows reference subject R_R1 with only one synergy and very similar values for both arms. Instead, patient P_7's data is decomposed with four synergies. The aided left side has high values for almost every muscle (these plots are normalized to 1 in order to compare synergies more easily). For excercise CO (figure A.23) two synergies are needed for reference subject's left side. As before, the values for both sides are similar. Again, patient P_7 has four synergies, that are hard to interprete. All muscles are involved in some way for both sides, during aided and non-aided excercises. Instead of nearly no muscle activation in the forearm, as the reference subject shows, patient P_7 has high contributions for BR and FCR.

With the help of these plots it is possible to analyze the synergies in a similar way as in subsection 4.2. Still, when having more than two synergies, those plots get crowded and difficult to comprehend. Then again, sorting synergies by their similarity could improve the way of representing (but not further investigated in this scope). But not only that, negative synergy values are hard to relate to muscle activation like in figure 11. However, inspecting the results for those two subjects and excercises already conveyed, that they correlate to the results seen in subsection 4.2.

### A.5.3. Analysis for the Numbers of Synergies

To further investigate the correlations between NMF and PCA, the number of synergies are compared and plotted for all subjects and excercises in figures A.24 to A.29 using PCA and figures A.30 to A.35 using NMF.

In general, the results are very similar: Reference subjects have fewer synergies than patients, P_7 has more synergies on his right side, the maximal number of synergies is around four to six and reference subjects have mainly about one to two synergies. An exception is excercise RF where the references' numbers of synergies are as high as the patients'. This can be due to the low signal to noise ratio already noted previously.

Yet, there are particular results that differ between PCA and NMF, e.g., excercise CF for patient P_7 has the same number of synergies (left: 2, right: 4) doing aided and non-aided excercises using PCA, whereas they are different for NMF. Furthermore, reference subjects' number of synergies are around 1 more fre-

quent using NMF.

### A.5.4. Evaluation of Synergy Patterns

In general, there is no evident result to identify the more suitable decomposition method for EMG signals. Rather, analyzing the patterns using NMF becomes more intuitive and easy, because of its non-negativity feature. Hence, their patterns can be examined easily for all excercises depicted in figures A.36 to A.41. These results show overall stable and reproducable patterns for within one reference subject. Across several subjects individual differences are possible, e.g., subject `R_P` also utilizes the biceps to do excercise `UAF` (figure A.36), whereas `R_R` mostly uses the deltoid. However, pattern changes have already been discussed in subsection 4.2.

After analyzing the number of synergies and synergy patterns, it becomes clear, that patients with a nearly uniform muscle pattern also have a high number of synergies. In order to decompose white noise, more synergies are needed (e.g. seen in figure A.19) and since no distinctive feature is present, synergies contribute in the same way for all muscles. This is not only true for patients, also reference subjects can have more uniform pattern due to little required muscle activity, e.g. like in excercise `RF` (see figure A.40). This leads to a higher number of synergies, too.

In sum, this subsection showed, that both, PCA and NMF, perform similarly, but due to the non-negativity feature of NMF, it is more convenient to visualize and interprete. The excercise `RF` showed comparatively bad results because of its low muscle activation. More synergies are needed and the low amplitude produces unfeasible synergy patterns for both, patients and reference subjects.

## A.6. Tracking with Depth Data

To be able to evaluate new methods and compare them with each other, an evaluation criterion is required. This criterion can be a comparism to ground truth data with the computed results.

In case of movement analysis useful ground truth data can be, e.g., the position at each timestep. As introduced in chapter 3, data recordings also included a depth videostream from Microsoft's Kinect. With this it is possible to extract the position of each limb in 3D space.

Position extraction is performed after the data was recorded. Thus, using online algorithms that need calibration like standing in phi-pose (Jean, 2012) are not applicable. Therefore, a simple approach was developed to extract 3D position of limbs from a depth videostream and is introduced in the next sections. This section will use the following notation:

| | |
|---|---|
| $P$ | a point in 2D or 3D euclidean space |
| $v$ | a position or state vector in state space |
| $\overrightarrow{v}$ | a vector with a defined direction |

### A.6.1. Human Model

The human model is based on six joints, three for each arm. A joint is represented as a point in the 3D space. The point can be extracted from a 2D depth image by camera calibration (Hartley & Zisserman, 2003). The three joints for one side are *wrist*, *elbow* and *shoulder*. They form a kinematic chain. *Shoulder* is the only joint that is fixed during tracking. Consequently, movement of the tracked person itself cannot be recognized. However, due to the experimental setup, it is assumed as neglectable. Furthermore, the elbow and wrist positions are restricted to the surface of a sphere defined by a radius (representing the length of the upper arm, respectively the forearm) and center point (represented by the previous joint in the kinematic chain). Figure A.5 shows a screenshot were each joint is marked as a blue colored circle.

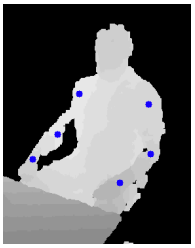

Fig. A.5: Screenshot were each joint is marked by blue colored circle

### A.6.2. Model of Table

The table is modelled as a plane, that can be defined by three points, composing two 2D-vectors: $\overrightarrow{v_d}$, $\overrightarrow{v_w}$, as depicted in figure A.6. Knowing the depth value of those three points, it is possible to model a plane and linearly interpolate the depth value for every point.

An arbitrary point on the plane $Z = (z_x, z_y)^T$ can be expressed by the linear combination of $\overrightarrow{v_d}$ and $\overrightarrow{v_w}$:

$$Z = x\frac{\overrightarrow{v_d}}{\|\overrightarrow{v_d}\|} + y\frac{\overrightarrow{v_w}}{\|\overrightarrow{v_w}\|} \tag{A.6}$$

$$Z = \begin{bmatrix}\overrightarrow{v_d}/\|\overrightarrow{v_d}\| & \overrightarrow{v_w}/\|\overrightarrow{v_w}\|\end{bmatrix}\begin{bmatrix}x\\y\end{bmatrix} \tag{A.7}$$

$x$ and $y$ represent the ratios of vectors $\overrightarrow{v_d}$ and $\overrightarrow{v_w}$ required to describe the point $Z$. Knowing the coordinates of $Z$ it is possible to compute $x$ and $y$ by recomposing equation A.7:

$$\begin{bmatrix}x\\y\end{bmatrix} = \begin{bmatrix}\overrightarrow{v_d}/\|\overrightarrow{v_d}\| & \overrightarrow{v_w}/\|\overrightarrow{v_w}\|\end{bmatrix}^{-1} Z \tag{A.8}$$

With the help of ratios $x$ and $y$ the depth value can be interpolated. To do that, the depth values at points $p_1$ ($p_{1,z}$) and $p_2$ ($p_{2,z}$) are needed:

$$Z_z = \frac{x\Delta d_z}{\|\overrightarrow{v_d}\|} + \frac{y\Delta w_z}{\|\overrightarrow{v_w}\|} + P_{1,z} + P_{2,z}, \tag{A.9}$$

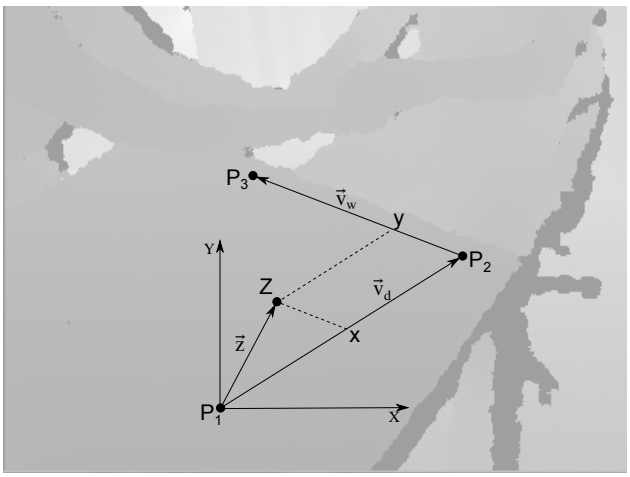


Fig. A.6: Depth image, overlayed by model of a table. Model allows to calculate the depth of an arbitrary point $Z$

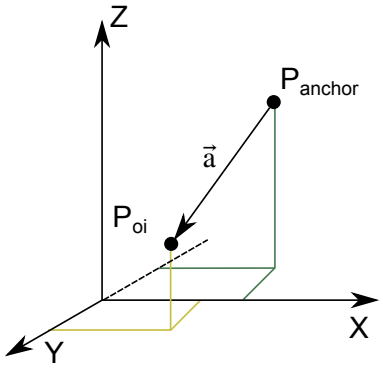


Fig. A.7: Illustration of two joints and their relation considered by the motion model

where $\Delta d_z = P_{2,z} - P_{1,z}$ and $\Delta w_z = P_{3,z} - P_{2,z}$.

### A.6.3. Motion Model

Modelling the natural motion of human arm joints with a euclidean linear model like $v = t/s, a = \text{const.}$ is not sufficient. The endeffector does not move linearly in euclidean space. Subsequently, the motion can be described more accurately with a motion model based on joint angles.

Each joint has its own motion model that takes track of the state, transition from one timestep to the next and its constraints. To get all information about the tracked joint $P_{\text{oi}}$ (point of interest), $P_{\text{anchor}}$ — the previous joint — is also needed. With the help of $P_{\text{anchor}}$ it is possible to set the center point of $P_{\text{oi}}$'s circular motion. That means if, e.g., the upper arm moves, the movement is centered around the shoulder joint. Both joints and their relations are illustrated in figure A.7.

Both joint positions are in cartesian space. But, as previously clarified, the motion model is based on angles: The state of a joint is described by $p = (\alpha, \beta)^T$, the transition from timestep $t-1$ to $t$ is $\overrightarrow{v} = (\Delta\alpha, \Delta\beta)^T$, and its constraints are the fixed length $r$ from joint $p$ to $p_{\text{oi}}$ and the maximum velocity $\overrightarrow{v}_{\max} = (v_\alpha, v_\beta)^T$.

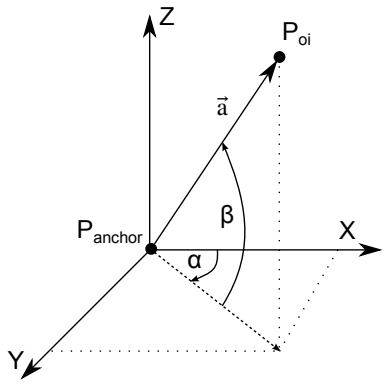


Fig. A.8: State of $p_{\text{oi}}$ is described by two angles: rotation around z-axis by $\alpha$, rotation around new defined y-axis by $\beta$ (yaw and pitch)

Figure A.8 depicts how state $p$ is derived.

In order to transform the cartesian coordinates to the state's $\alpha$ and $\beta$, the function `atan2` can be used. It is a compact way to determine the angle between a vector and a reference. With the help of `atan2` (GNU, 2014) state $p$ can be computed by

$$p = \begin{pmatrix} \alpha \\ \beta \end{pmatrix} \tag{A.10}$$

$$= \begin{pmatrix} \text{atan2}(\text{y}_{\text{oi}}, \text{x}_{\text{oi}}) \\ \text{atan2}(\text{z}_{\text{oi}}, \|(\text{x}_{\text{oi}}, \text{y}_{\text{oi}})^{\text{T}}\|) \end{pmatrix}, \tag{A.11}$$

where $(x_{\text{oi}}, y_{\text{oi}}, z_{\text{oi}})^T = P_{\text{oi}}$ in cartesian coordinates. Transforming back from state space to cartesian space is done by

$$P_{\text{oi}} = r \begin{pmatrix} \cos\alpha \cos\beta \\ \sin\alpha \cos\beta \\ \sin\beta \end{pmatrix}. \tag{A.12}$$

The movement is modelled as a linear change in angles. Only the difference between the angles of two consecutive timesteps is captured. No higher order interpolation is done, because the stepsize is relatively small compared to the recorded movement. Due to the fact, that the function `atan2` returns values in range $-\pi \ldots \pi$, jumps in $\overrightarrow{v}$ can occur, that have to be taken into account.

The general procedure of the motion model is as follows:
As a new frame arrives, the state of the corresponding motion model of joint $P_{\text{oi}}$ has to be updated. The joint is transformed into the state space and $\overrightarrow{v}$ is directly calculated by $s_t - s_{t-1}$. To smooth the motion of this joint, the mean of the previous and current $\overrightarrow{v}$ is computed and used to calculate the new state of the motion model. Those steps are only sufficient for the last joint in the kinematic chain, the wrist. In case of the elbow (and shoulder, if it would be modelled), all subsequent joints need to be adjusted. Disregarding the issue will lead to a wrong representation of the subsequent joints as it is illustrated in figure A.9a.

To take care of that situation, the joint $p_{wrist}$ needs to be updated by $\overrightarrow{v}$ just like the elbow. The result can

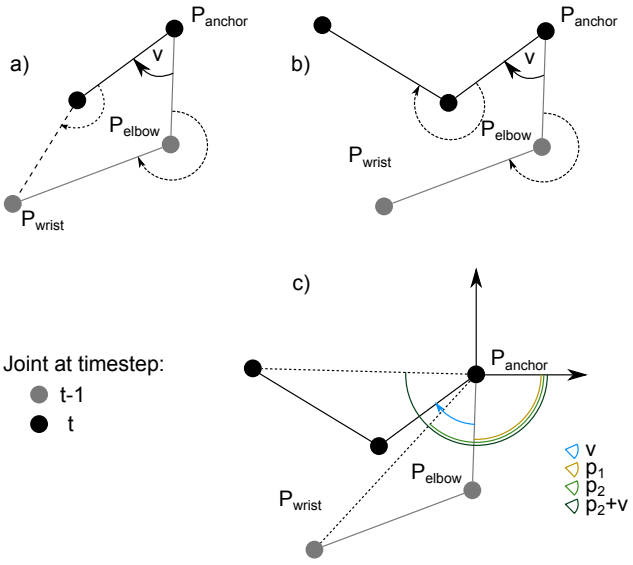


Fig. A.9: Visualizing the concept of projecting the wrist position, for simplification only in 2D, a) if no projection is done, the state of wrist is changing even though only the state of elbow changed, b) state of wrist is not changing because wrist position is projected according to the change of state in elbow, c) showing angles to calculate the projection

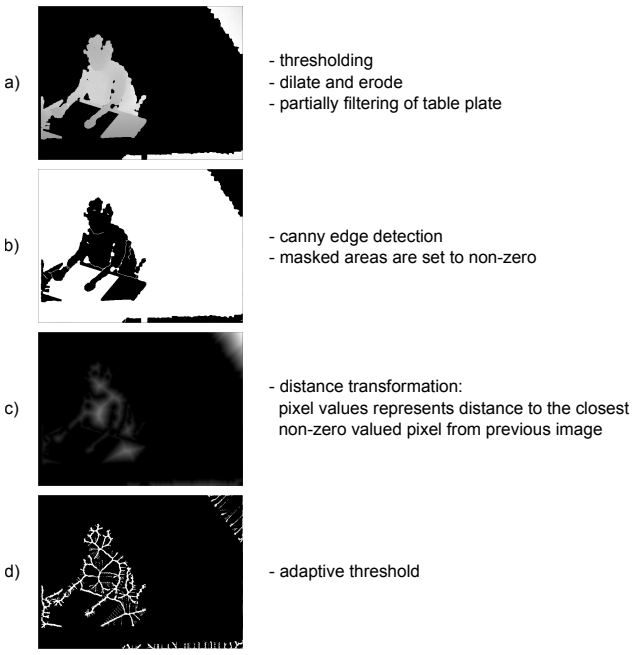


Fig. A.10: Showing intermediate results of approach

be seen in figure A.9b. Differently expressed, $P_{wrist}$ is rotated around $P_{\text{anchor}}$ by $\overrightarrow{v}$. In the state space of the elbow joint this reduces to $p_2 + \overrightarrow{v}$ as it can be seen in figure A.9c.

### A.6.4. Approach

Before the the algorithm can automatically track the limb position, several user inputs are required:

- thresholds for far and near distances
- 3 points to define the plane of the table
- initial position of each human joint

The threshold-mask is smoothed by erode and dilate filters (Soille, 2003) and used to reduce the search space. To enhance the quality of tracking during rest, it is necessary to also filter the table. Trying to filter by thresholding is not sufficient because it would also mask important features of the human. The table filter is designed according to appendix A.6.2 and restricted to a polygon previously defined by the user input to sample the depth data. The result of all applied user inputs can be seen in figure A.10 a.

The next goal is to transform the image into a binary image that represents a kind of skeleton. This can be achieved by using distance transformation (Borgefors, 1986) on a binary image. It will compute the distance to the nearest non-zero pixel for each pixel of the input image. To obtain such an input image as it is shown in figure A.10b, canny edge detection (Canny, 1986) is used on the masked depth image.

The distance transformation has the disadvantage that values can differ greatly, e.g. distances of the upper body can be greater than distances of the forearm as it is shown in A.10c. Forearm pixels are merely visible, whereas pixel of the upper body are relatively bright.

This is difficult to evaluate. Therefore, an adaptive threshold is used. It is independent of global distances and calculates the threshold based on local features (Gonzales & Woods, 1992). The method's output is, again, a binary image as A.10d shows. It is the basis for choosing points in the image as possible joint positions. That means, all zero valued points are excluded for the upcoming fitting process. Every joint is handled seperately and successively. At first, the joint position is predicted to the current timestep $t$ with the help of the motion model (see appendix A.6.3). This position is the center point of a window defining the search space for the actual, new joint position. To even further restrict the search, a point should be within a specified depth range. This set is further referred to as $\mathcal{C}$, where a specific point is depicted as $\mathcal{C}_i$, with $i = 0 \ldots N_{\mathcal{C}} - 1$ and $N_{\mathcal{C}}$ as the number of points in $\mathcal{C}$.

To finally select the best fit from the set of candidates $\mathcal{C}$, further calculations are done in 3D space. For this purpose a new set of points $\mathcal{P}$ is chosen. Again, a point of this set is referred to $\mathcal{P}_k$, where $k = 0 \ldots N_{\mathcal{P}} - 1$ with $N_{\mathcal{P}}$ as number of points in $\mathcal{P}$. Points for $\mathcal{P}$ are chosen by taking all valid points that reside inside the rectangle with upper and lower corners at the predicted and at the previous joint. It is assumed that all those points approximate the skeleton's forearm or upperarm respectively. That in turn can be simplified to a linear function in 3D. To find the function that is most

consistent with $\mathcal{P}$, $F(i)$ is defined by

$$F(i) = \sqrt{\sum_{k}^{N_P} \left( \frac{\|(\mathcal{P}_k - P_{\text{anchor}}) \times (\mathcal{C}_i - P_{\text{anchor}})\|}{\|(\mathcal{C}_i - P_{\text{anchor}})\|} \right)^2} \tag{A.13}$$

and $i$ is chosen so that $F(i)$ is minimized. A graphical summary is shown in figure A.11. In case there are no candidates to choose from, only the predicted position by the motion filter is used.

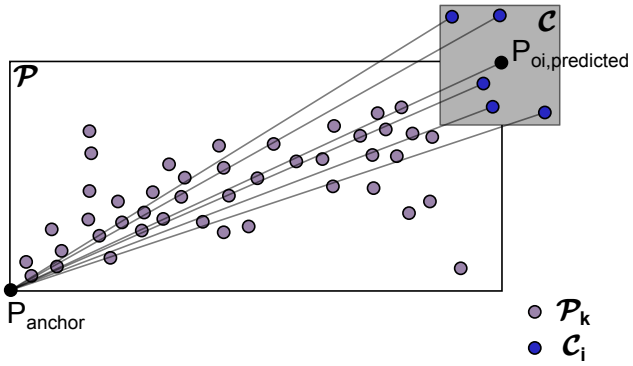


Fig. A.11: For every $i$ in $\mathcal{C}$ a linear function is defined by $P_{\text{anchor}}$ and $\mathcal{C}_i$ illustrated as gray lines. Equation (A.13) calculates the distance for every $\mathcal{P}_k$ to the corresponding linear function of $\mathcal{C}_i$.

### A.6.5. Limit of Approach

This chapter shows the limit of the algorithm and how it could be improved in the future.

Handling occlusion is partly achieved with the help of the motion model. It can extrapolate the position and motion of joints if they are temporally covered by other objects. Those objects must be at least 10cm apart from the tracked limbs. In case for objects too close or self-occlusion, the approach fails. Self-occlusion can happen when the person lifts his arm so that, for example, the forearm covers the upper arm.

A possibility to overcome that problem is to recognize self-occlusion and use backpropagation or a more detailed human model. This approach tried to avoid the issue by letting the user manually adjust each joint if necessary. But adjusting only one frame will not lead to better tracking results afterwards. As long as the problem remains, every frame with occlusion has to be taken care of.

### A.7. Images

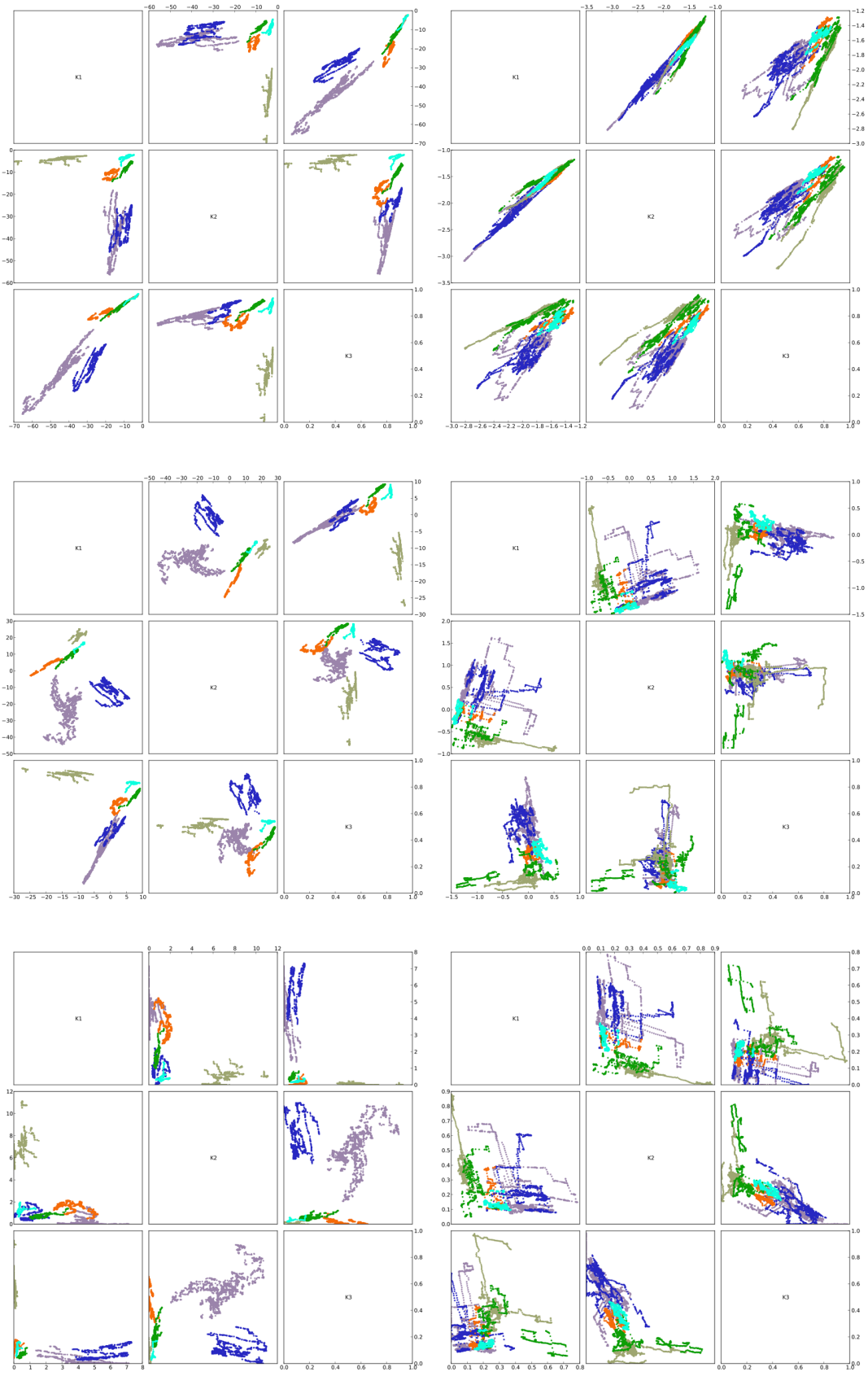


Fig. A.12: Dimensionality reduction of excercises shown in figure 3 for patient P_7, aided. Left column for left arm and right column for right arm. Each row represents a different dimensionality reduction technique, from top to bottom: GSK, PCA, NMF.

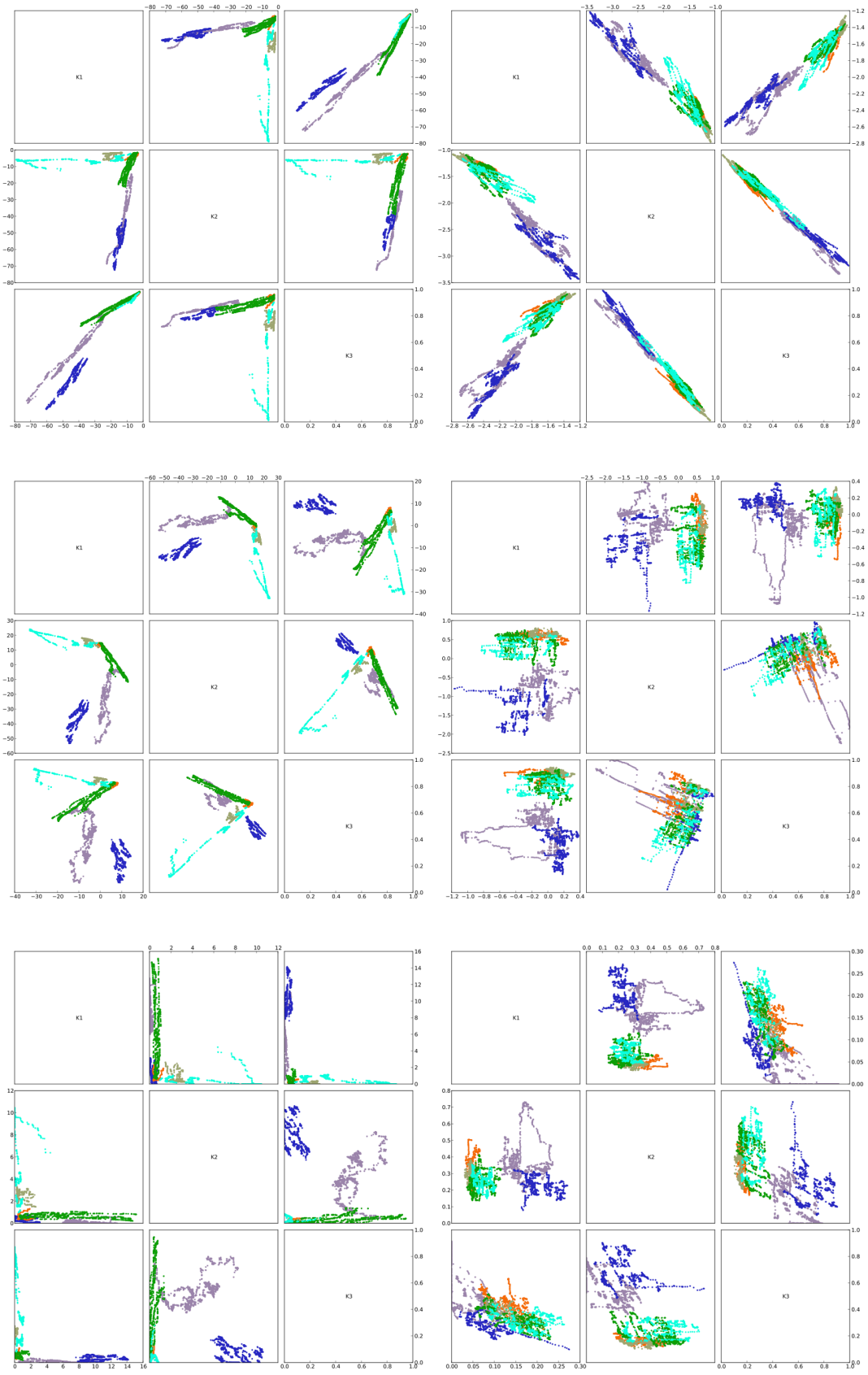


Fig. A.13: Dimensionality reduction of excercieses shown in figure 3 for patient P_7, non-aided. Left column for left arm and right column for right arm. Each row represents a different dimensionality reduction technique, from top to bottom: GSK, PCA, NMF.

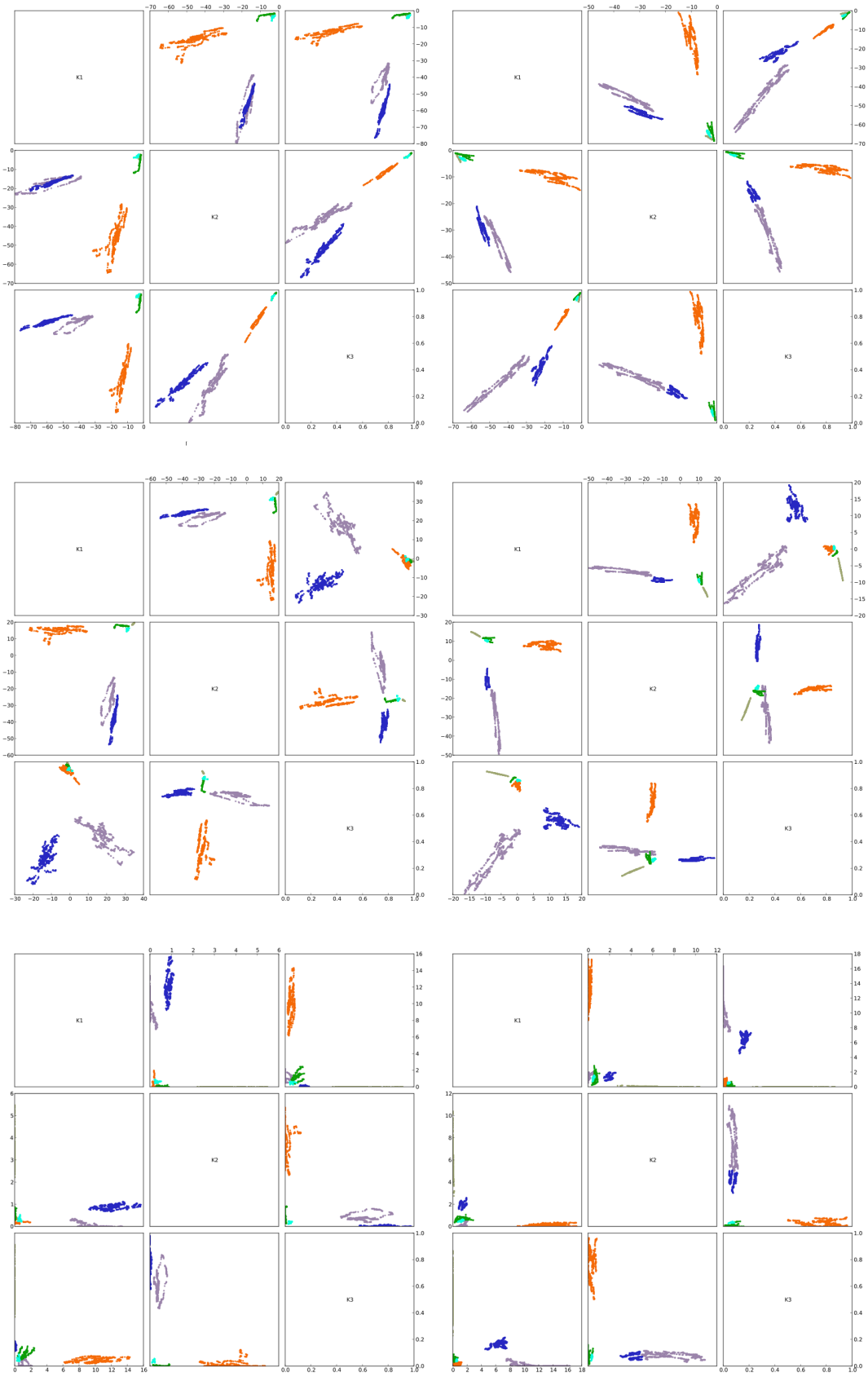


Fig. A.14: Dimensionality reduction of excercises shown in figure 3 for reference subject `R_R1`. Left column for left arm and right column for right arm. Each row represents a different dimensionality reduction technique, from top to bottom: GSK, PCA, NMF.

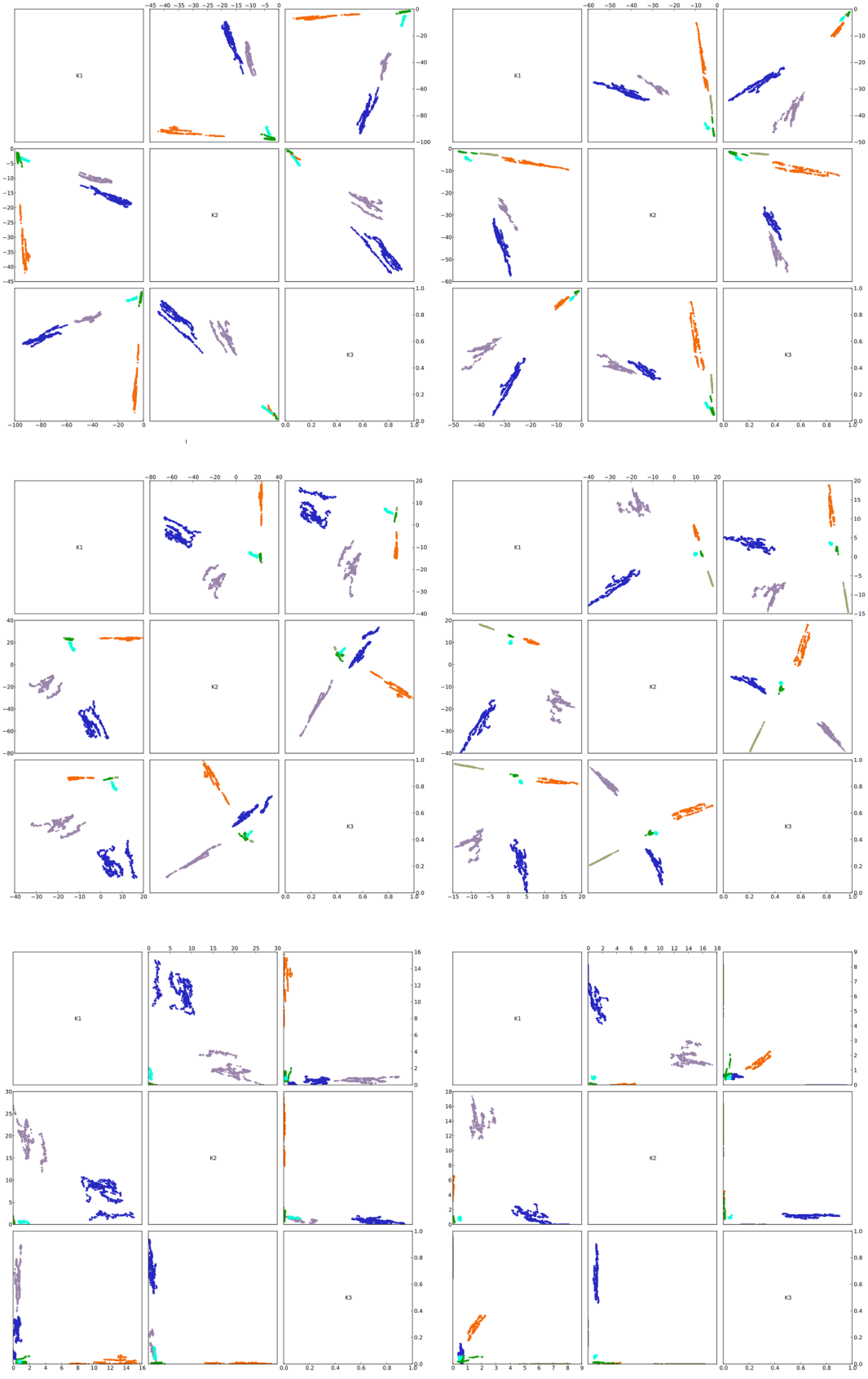


Fig. A.15: Dimensionality reduction of excercises shown in figure 3 for reference subject R_R2. Left column for left arm and right column for right arm. Each row represents a different dimensionality reduction technique, from top to bottom: GSK, PCA, NMF.

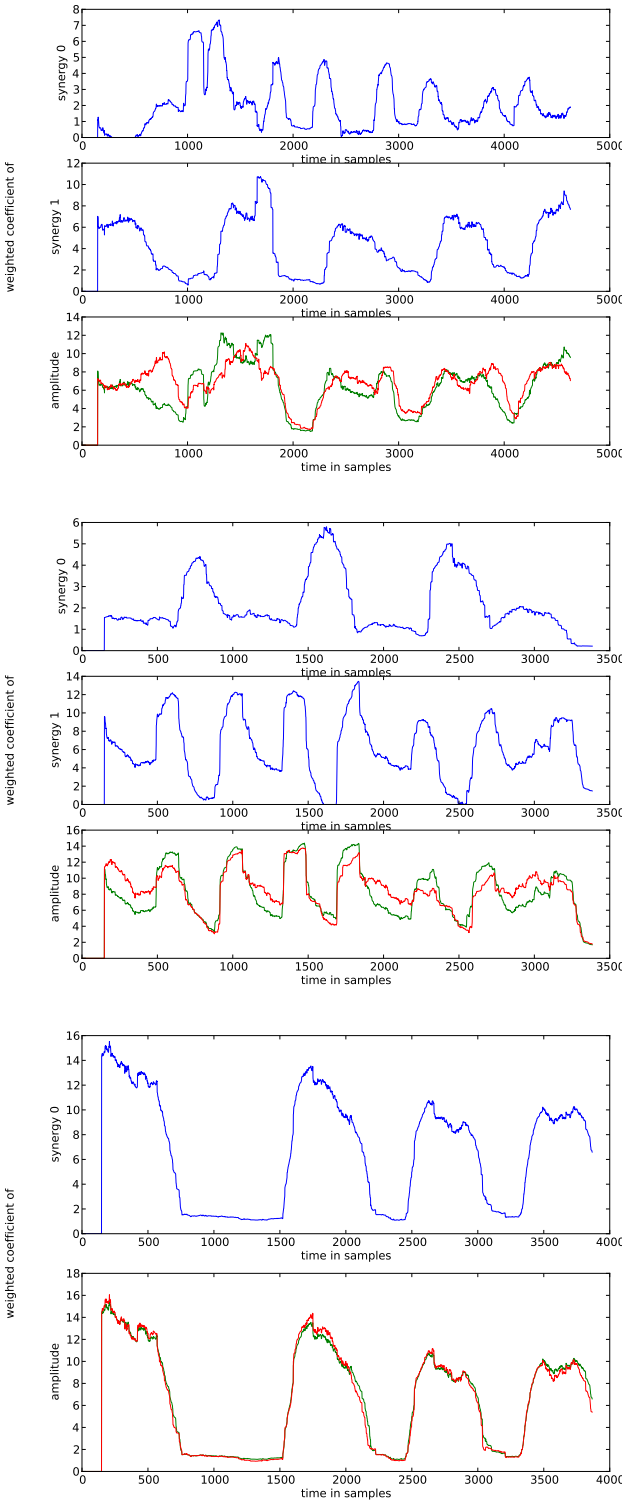


Fig. A.16: Muscle contribution of BR for excercise CF and left side with each reconstructed (green) and original (red) signal in last subplot. Subjects from top to bottom: P_7 aided, non-aided, R_R2.

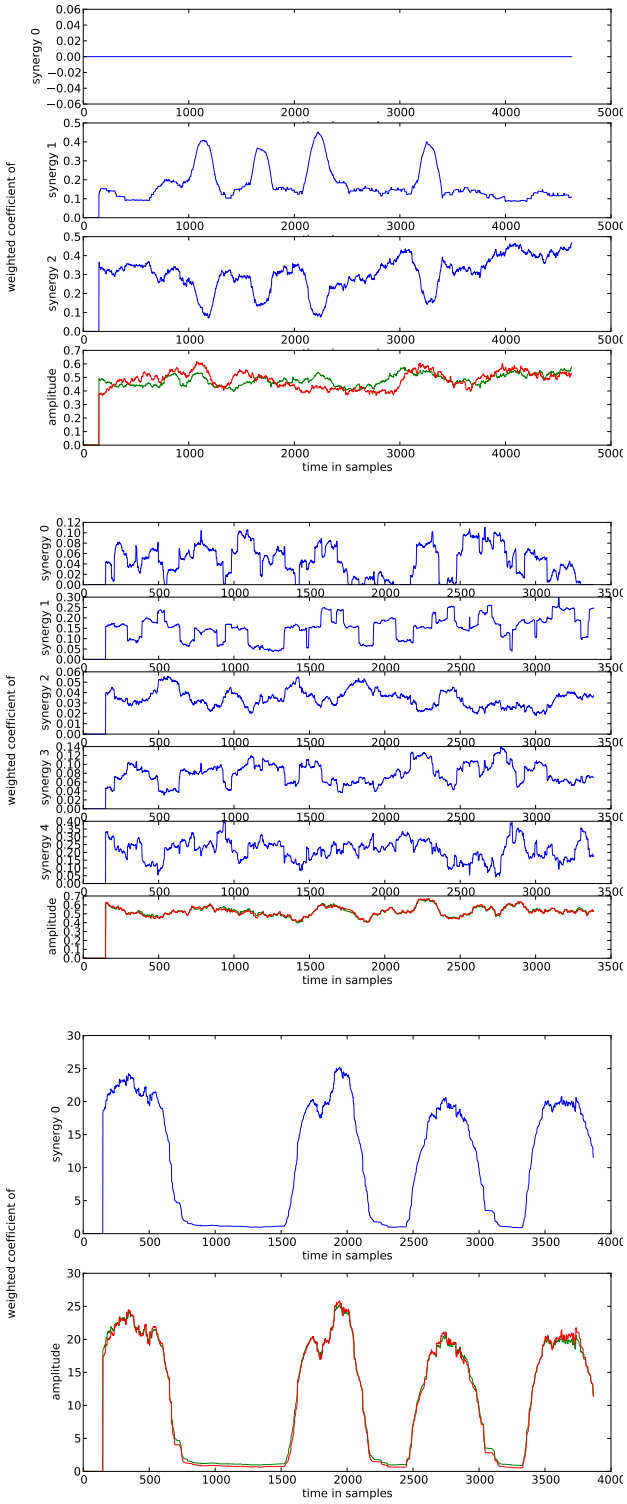


Fig. A.17: Muscle contribution of BR for excercise CF and right side with each reconstructed (green) and original (red) signal in last subplot. Subjects from top to bottom: P_7 aided, non-aided, R_R2.

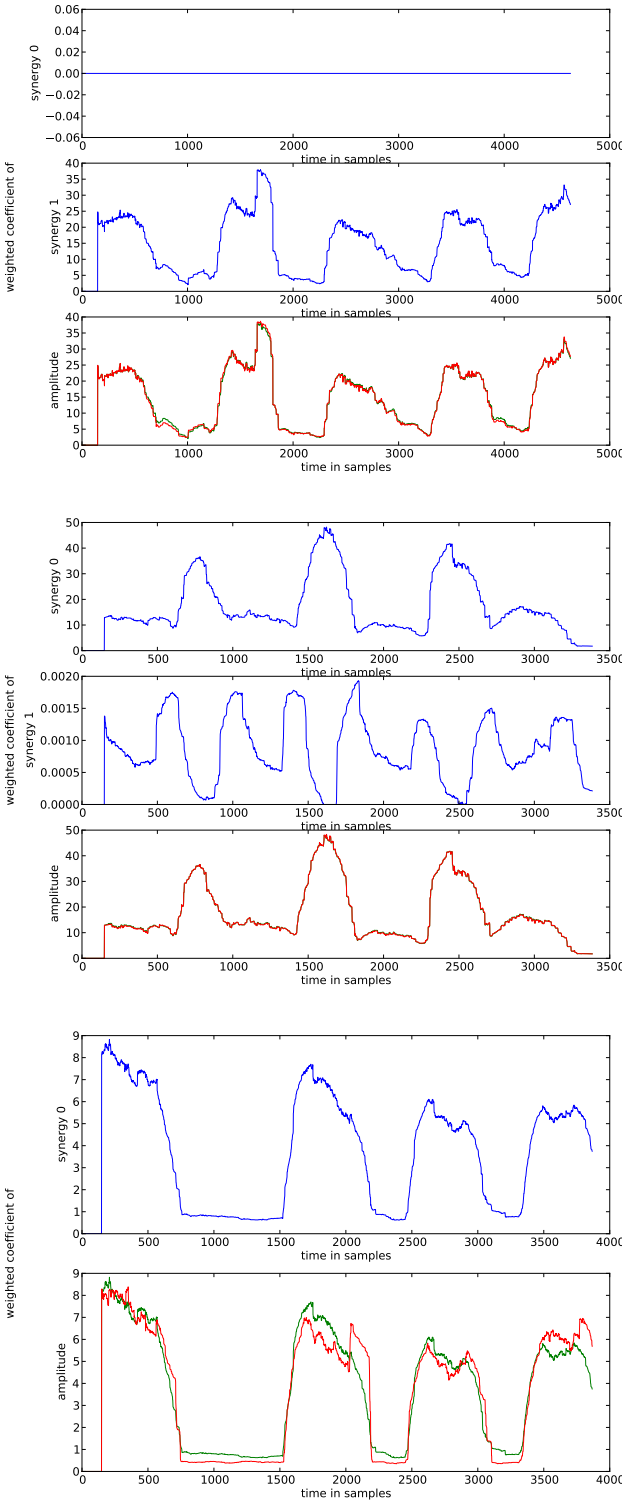


Fig. A.18: Muscle contribution of FCR for excercise CF with left side with each reconstructed (green) and original (red) signal in last subplot. Subjects from top to bottom: P_7 aided, non-aided, R_R2.

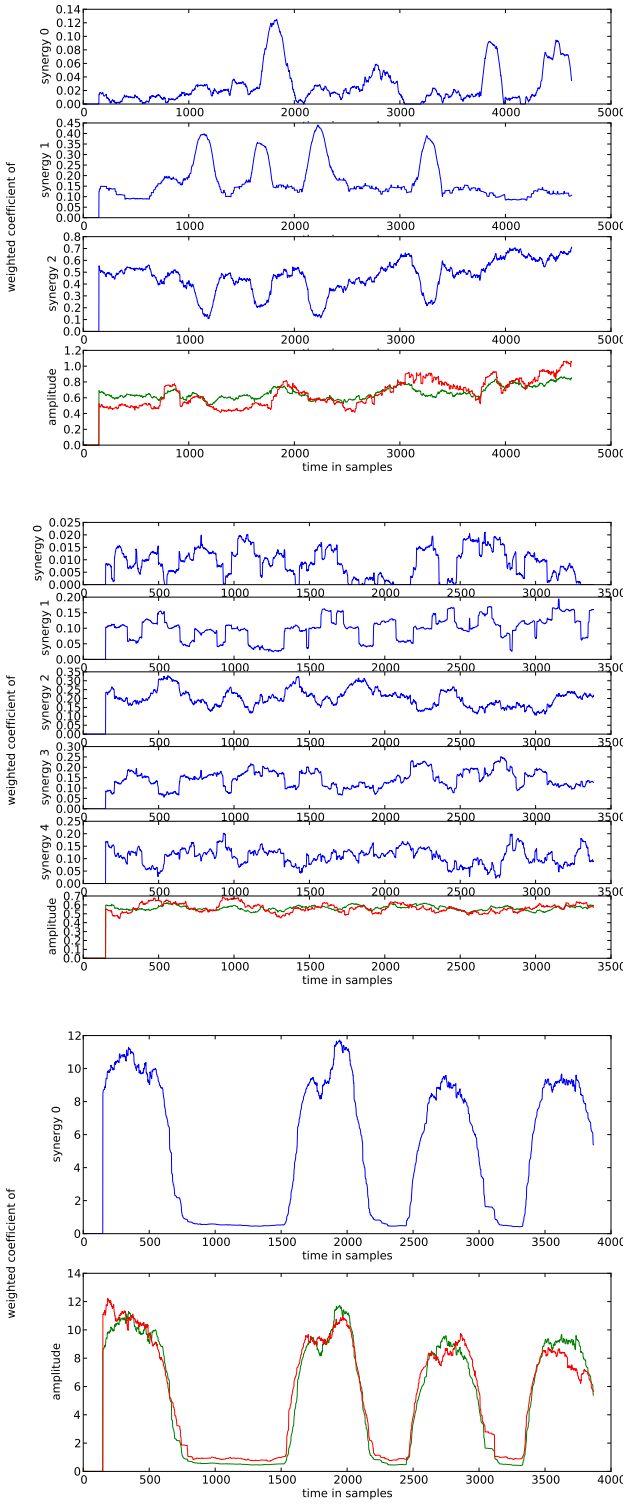


Fig. A.19: Muscle contribution of FCR for excercise CF with right side with each reconstructed (green) and original (red) signal in last subplot. Subjects from top to bottom: P_7 aided, non-aided, R_R2.

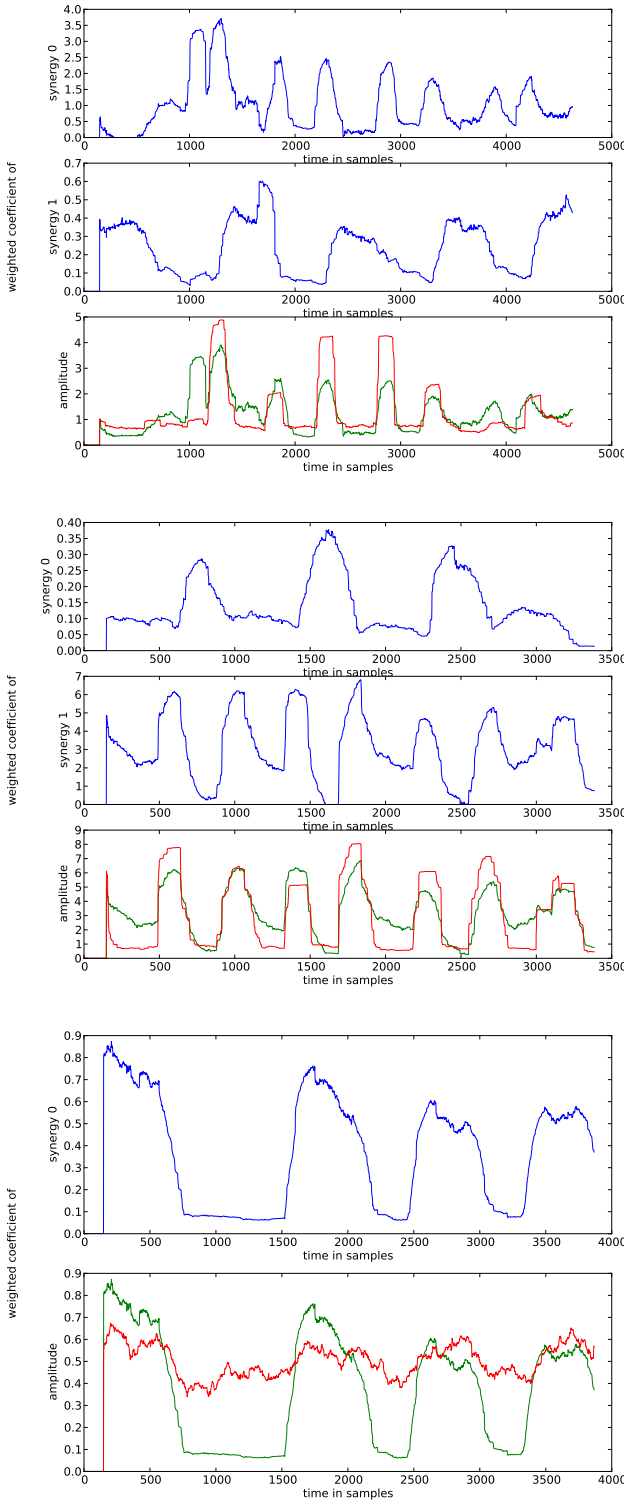


Fig. A.20: Muscle contribution of BSL for excercise CF with left side with each reconstructed (green) and original (red) signal in last subplot. Subjects from top to bottom: P_7 aided, non-aided, R_R2.

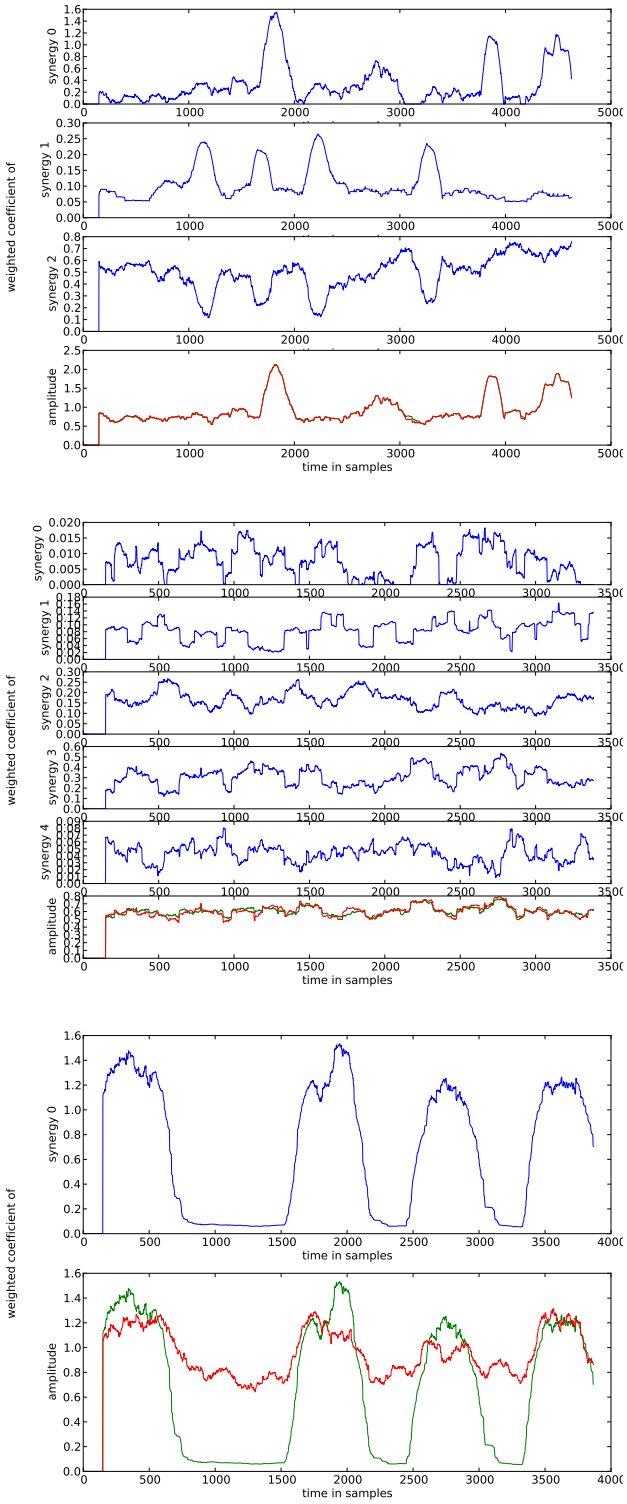


Fig. A.21: Muscle contribution of BSL for excercise CF with right side with each reconstructed (green) and original (red) signal in last subplot. Subjects from top to bottom: P_7 aided, non-aided, R_R2.

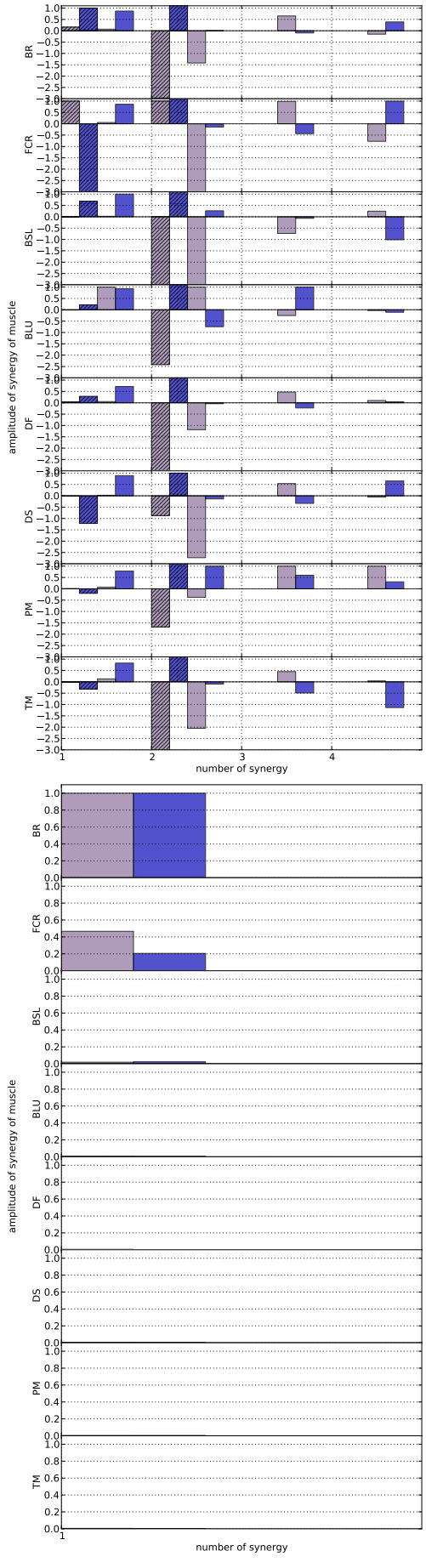


Fig. A.22: Synergies of excercise CF for every muscle calculated by PCA for patient P_7 (top) and reference subject R_R1, legend see figure 6

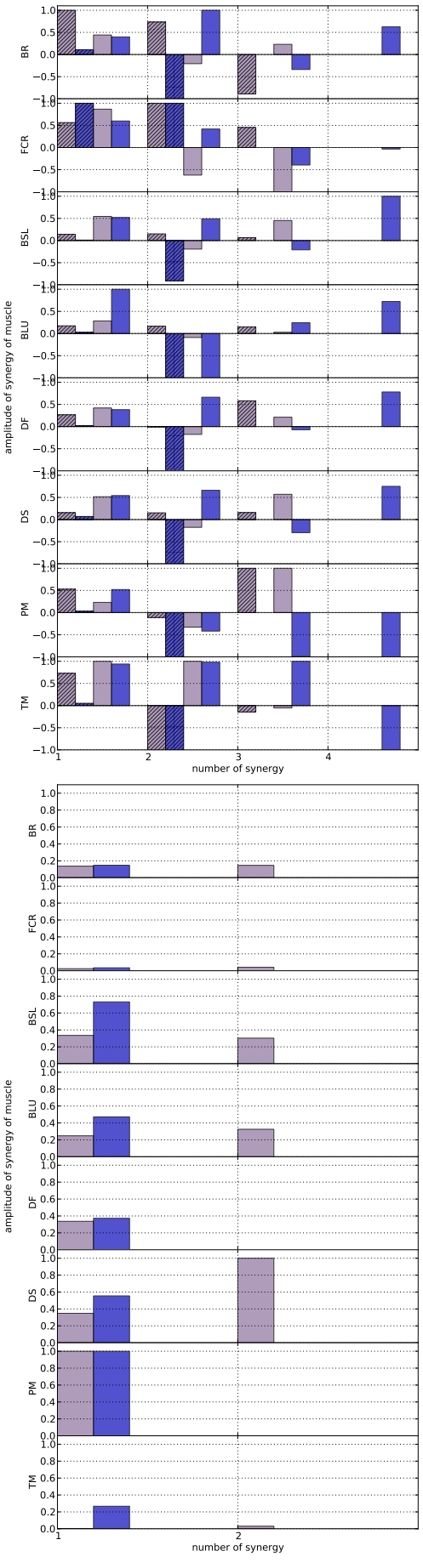


Fig. A.23: Synergies of excercise CO for every muscle calculated by PCA for patient P_7 (top) and reference subject R_R1, legend see figure 6

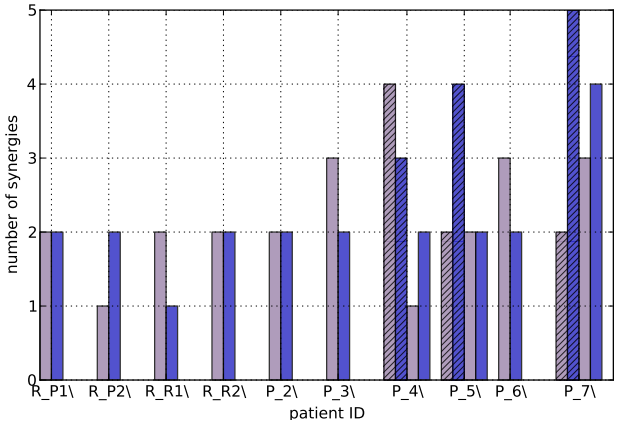


Fig. A.24: Number of synergies using PCA for excercise `UAF-90` for each patient and reference subject to reconstruct 95% of original signal, legend see fig. 6

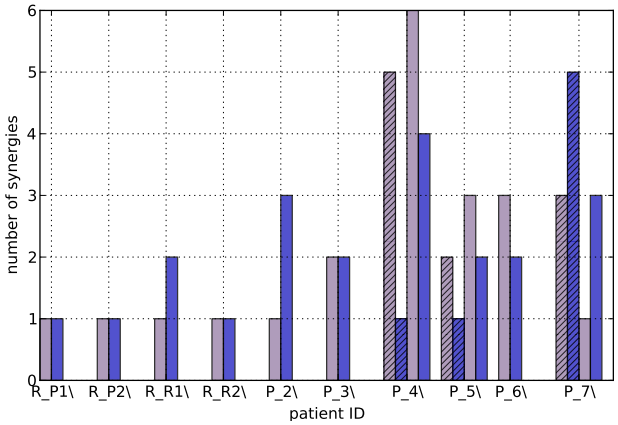


Fig. A.25: Number of synergies using PCA for excercise `UAS-90` for each patient and reference subject to reconstruct 95% of original signal, legend see fig. 6

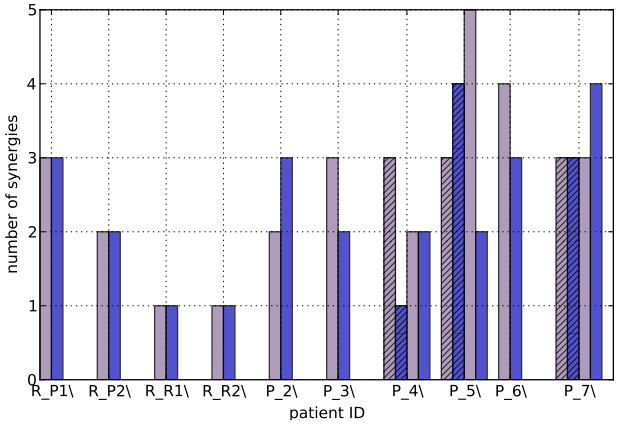


Fig. A.26: Number of synergies using PCA for excercise `AA-90` for each patient and reference subject to reconstruct 95% of original signal, legend see fig. 6

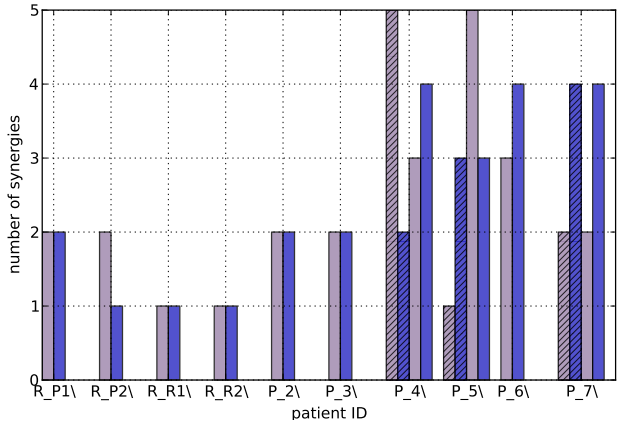


Fig. A.27: Number of synergies using PCA for excercise `CF` for each patient and reference subject to reconstruct 95% of original signal, legend see fig. 6

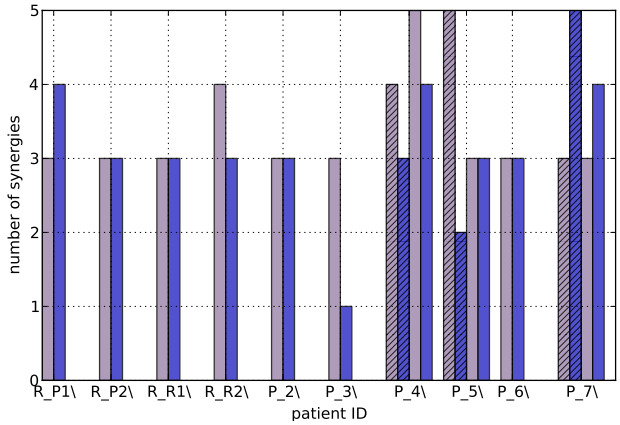


Fig. A.28: Number of synergies using PCA for excercise `RF` for each patient and reference subject to reconstruct 95% of original signal, legend see fig. 6

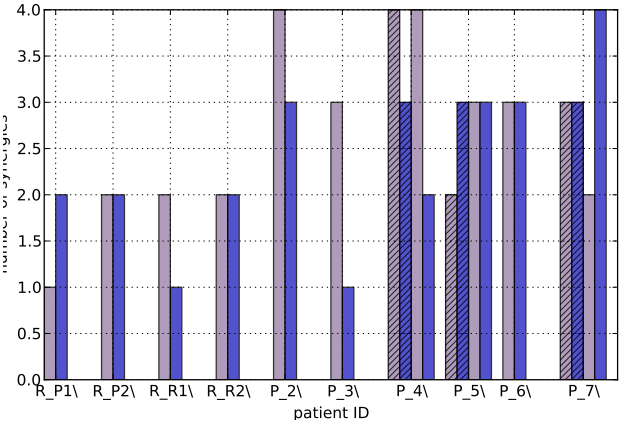


Fig. A.29: Number of synergies using PCA for excercise `CO` for each patient and reference subject to reconstruct 95% of original signal, legend see fig. 6

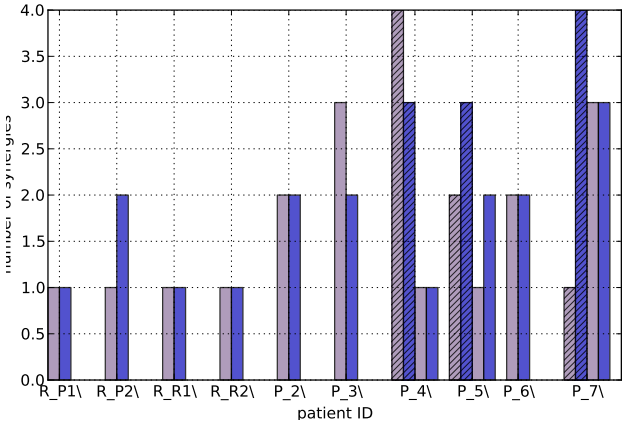


Fig. A.30: Number of synergies using NMF for excercise `UAF-90` for each patient and reference subject to reconstruct 95% of original signal, legend see fig. 6

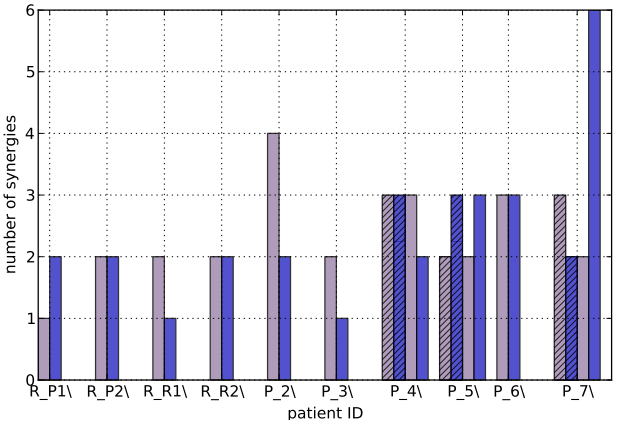


Fig. A.33: Number of synergies using NMF for excercise `CF` for each patient and reference subject to reconstruct 95% of original signal, legend see fig. 6

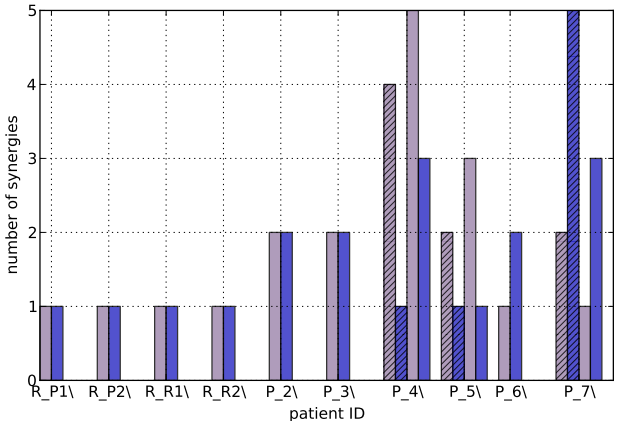


Fig. A.31: Number of synergies using NMF for excercise `UAS-90` for each patient and reference subject to reconstruct 95% of original signal, legend see fig. 6

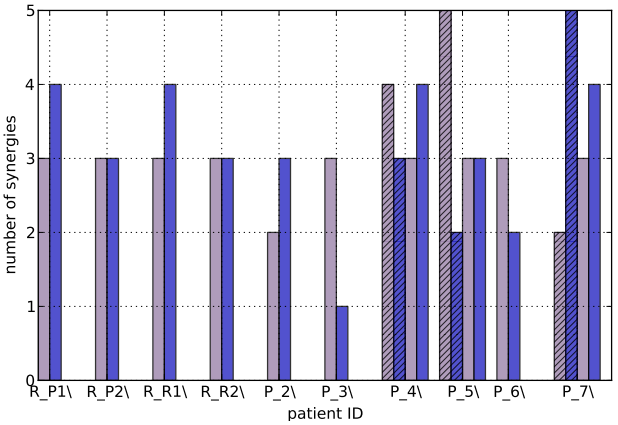


Fig. A.34: Number of synergies using NMF for excercise `RF` for each patient and reference subject to reconstruct 95% of original signal, legend see fig. 6

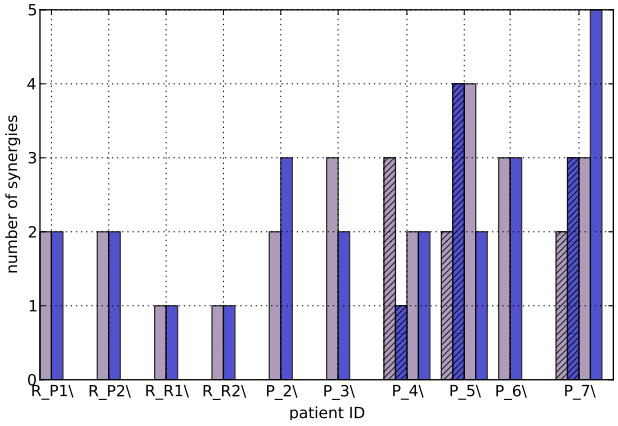


Fig. A.32: Number of synergies using NMF for excercise `AA-90` for each patient and reference subject to reconstruct 95% of original signal, legend see fig. 6

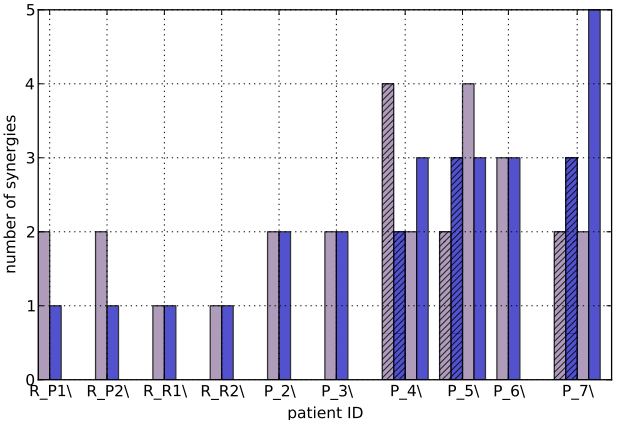


Fig. A.35: Number of synergies using NMF for excercise `CO` for each patient and reference subject to reconstruct 95% of original signal, legend see fig. 6

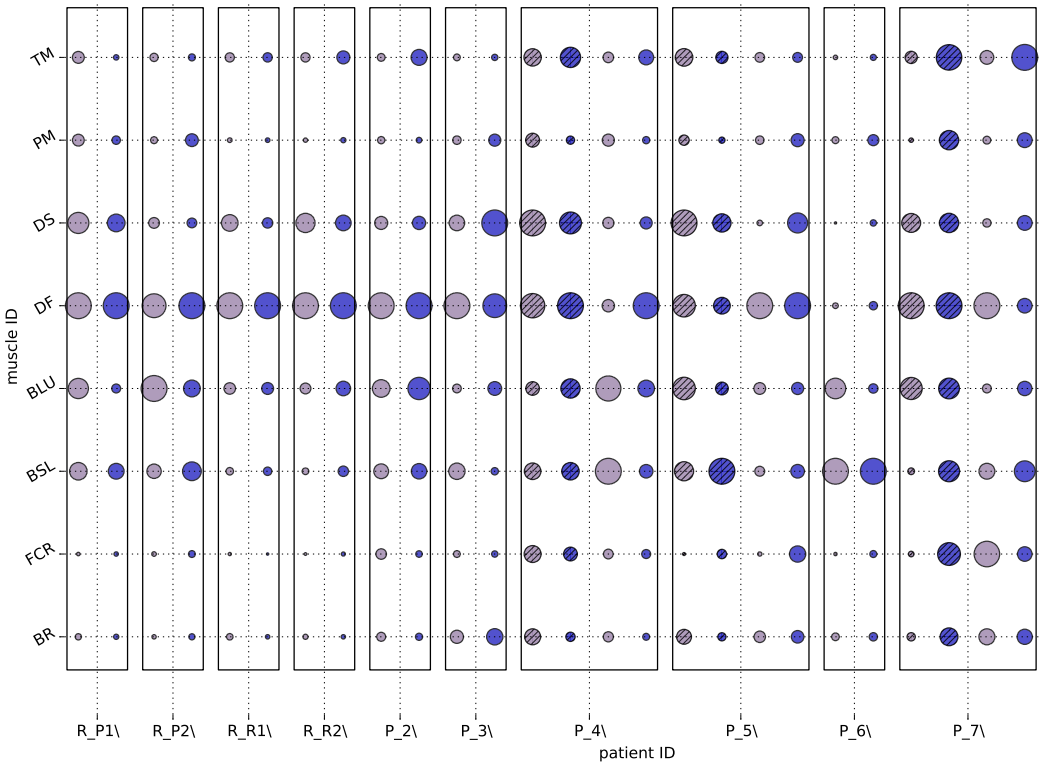


Fig. A.36: Muscle contribution for excercise `UAF` summed for each synergy and calculated by NMF, legend see fig. 6

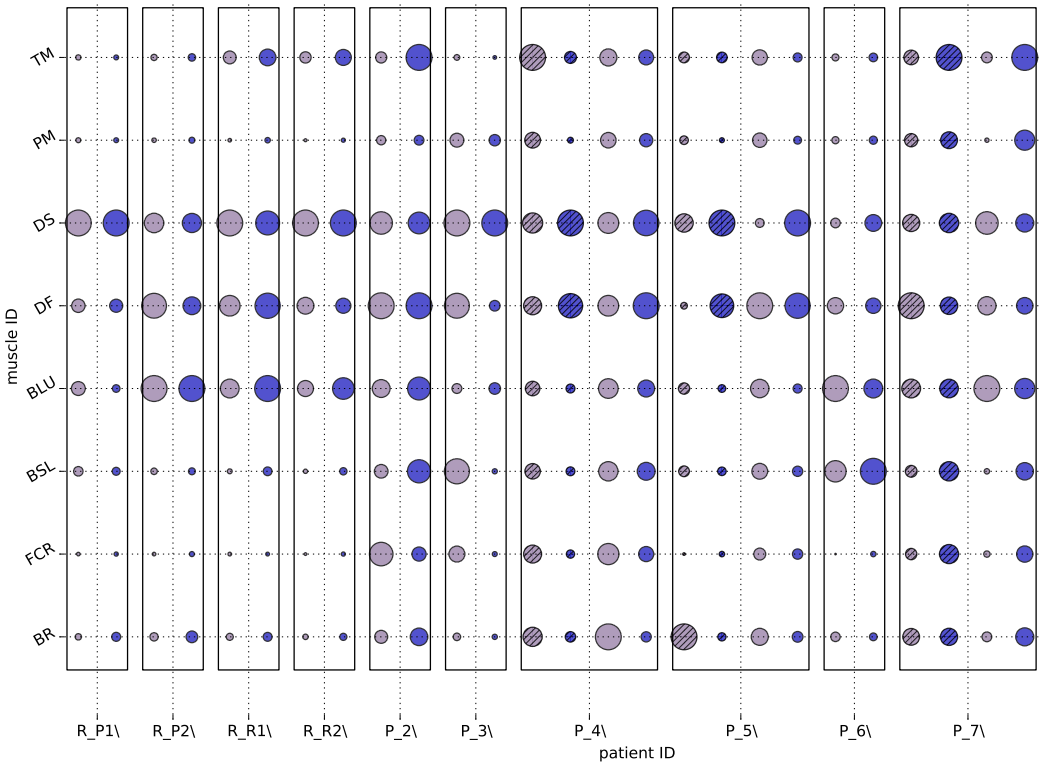


Fig. A.37: Muscle contribution for excercise `UAS` summed for each synergy and calculated by NMF, legend see fig. 6

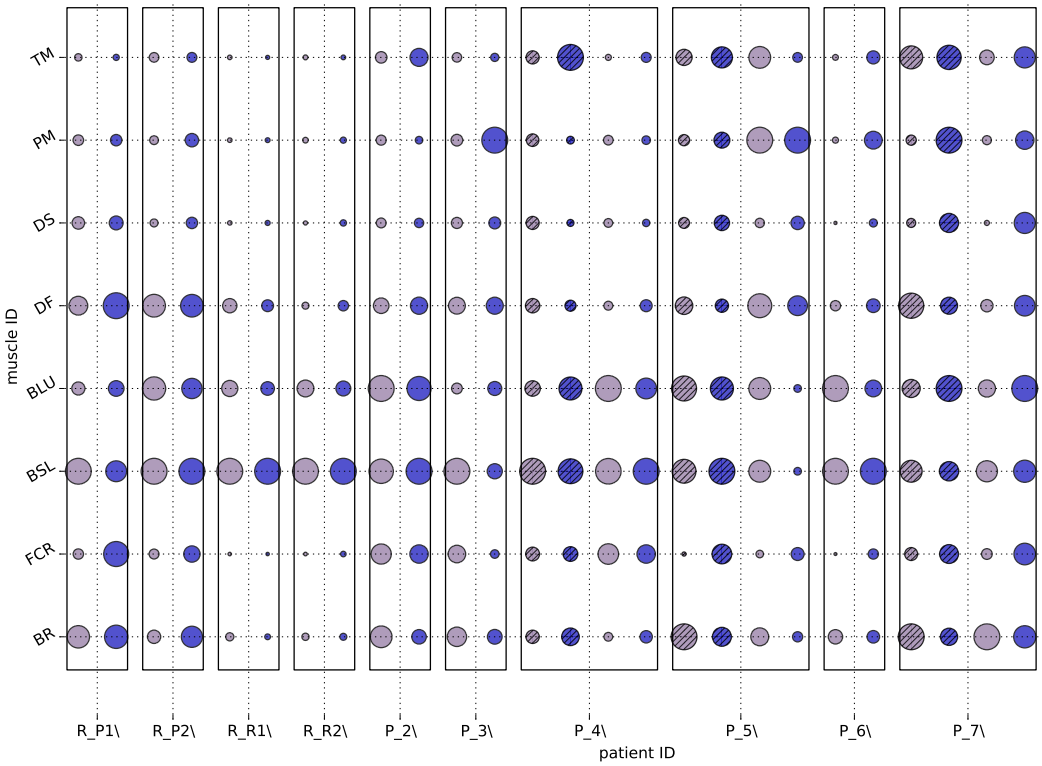


Fig. A.38: Muscle contribution for excercise `AA` summed for each synergy and calculated by NMF, legend see fig. 6

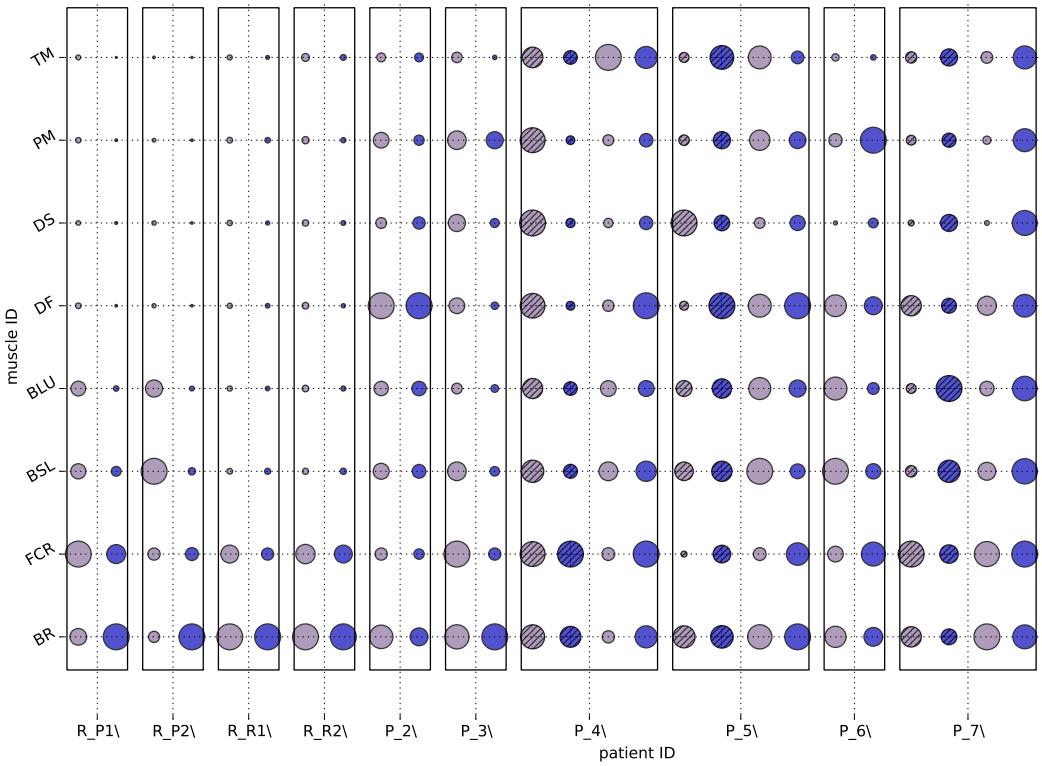


Fig. A.39: Muscle contribution for excercise `CF` summed for each synergy and calculated by NMF, legend see fig. 6

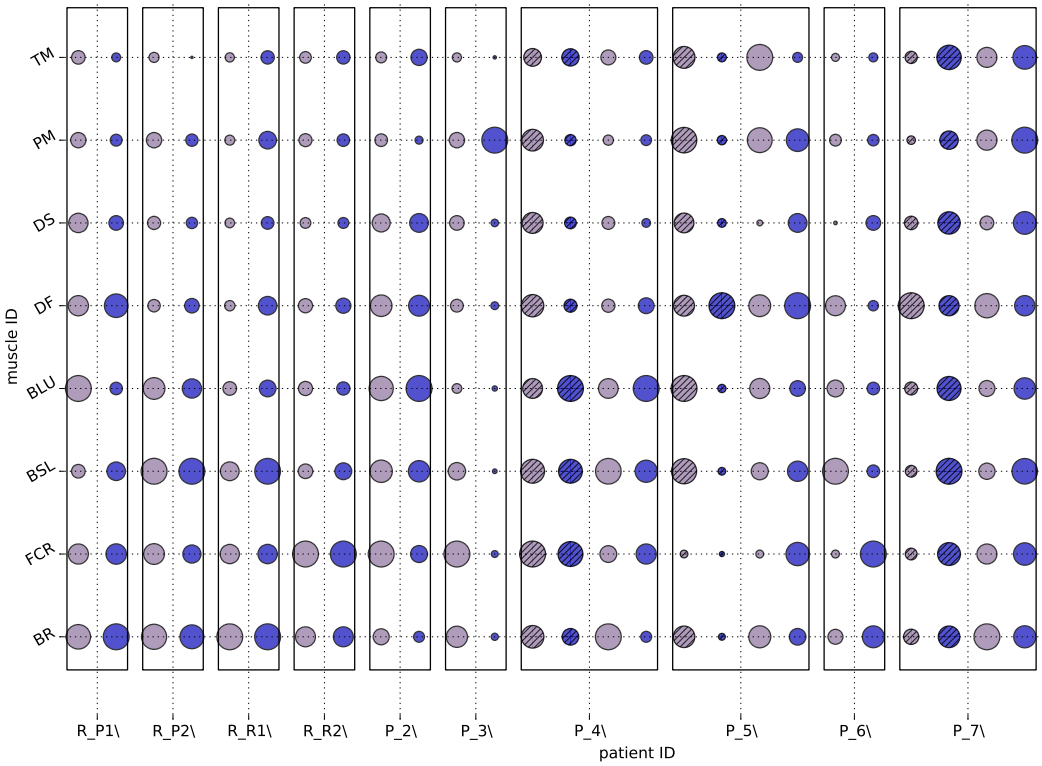


Fig. A.40: Muscle contribution for excercise `RF` summed for each synergy and calculated by NMF, legend see fig. 6

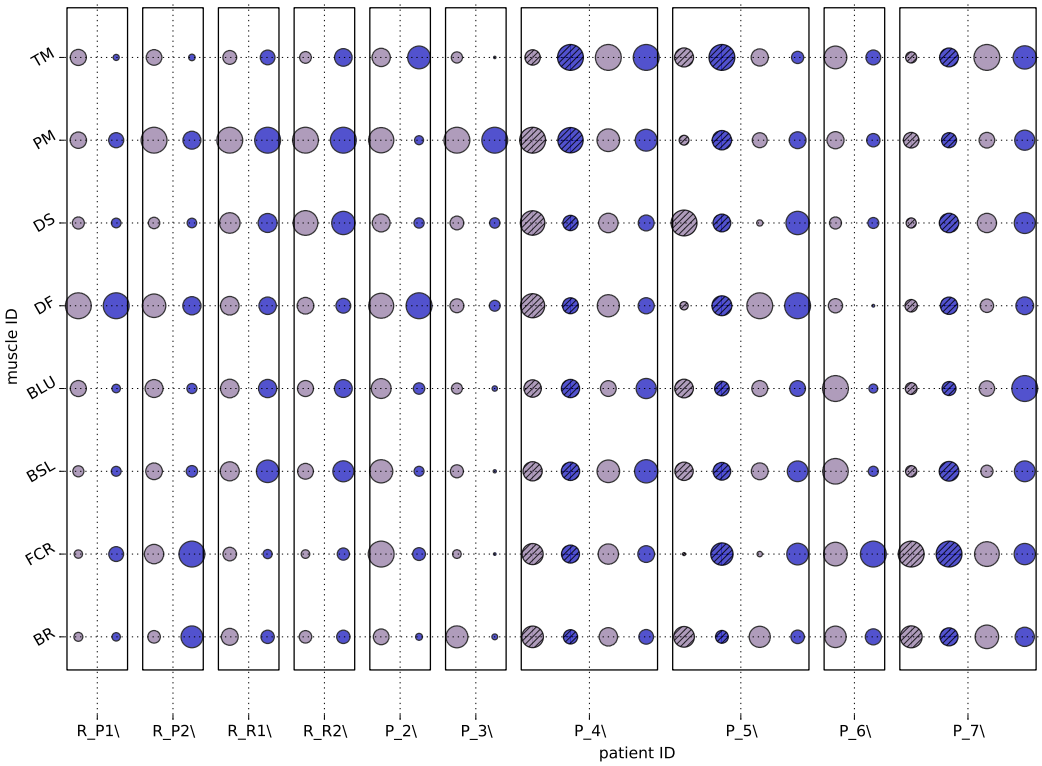


Fig. A.41: Muscle contribution for excercise `CO` summed for each synergy and calculated by NMF, legend see fig. 6

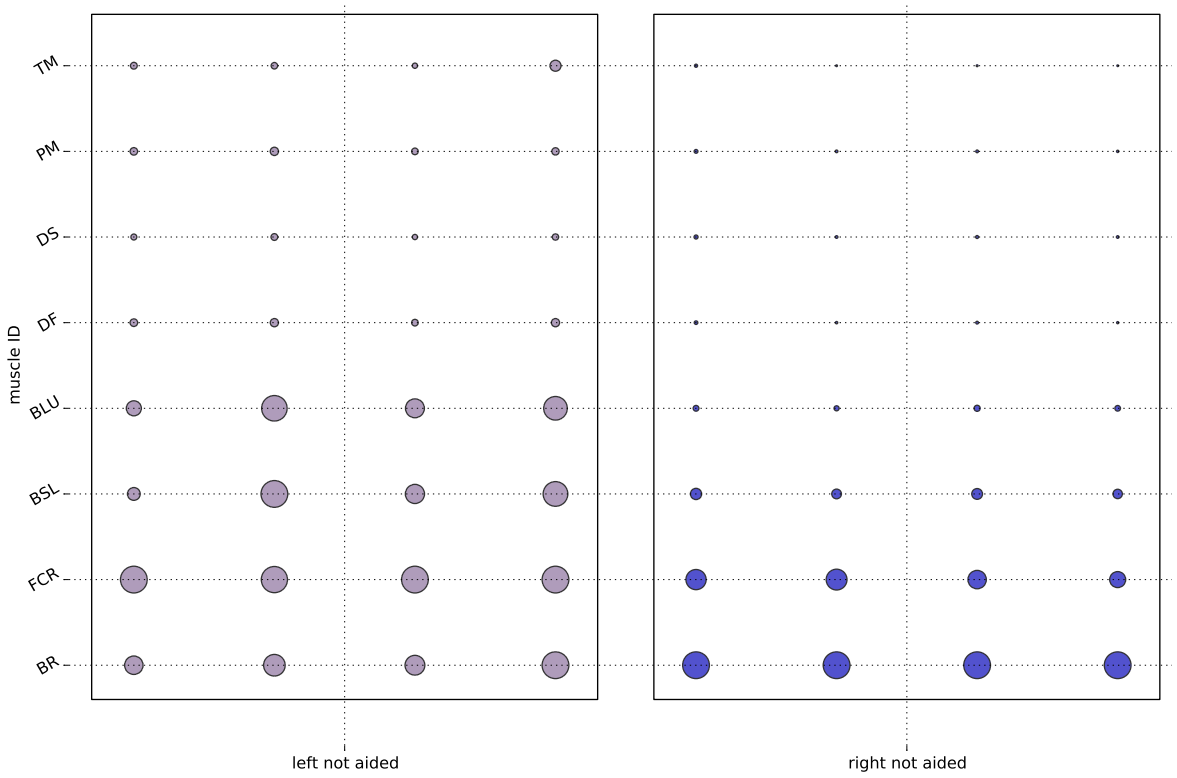


Fig. A.42: Muscle contribution summed for each synergy and calculated by NMF for every repetition during excercise `CF` of reference subject `R_R1`, legend see fig. 6

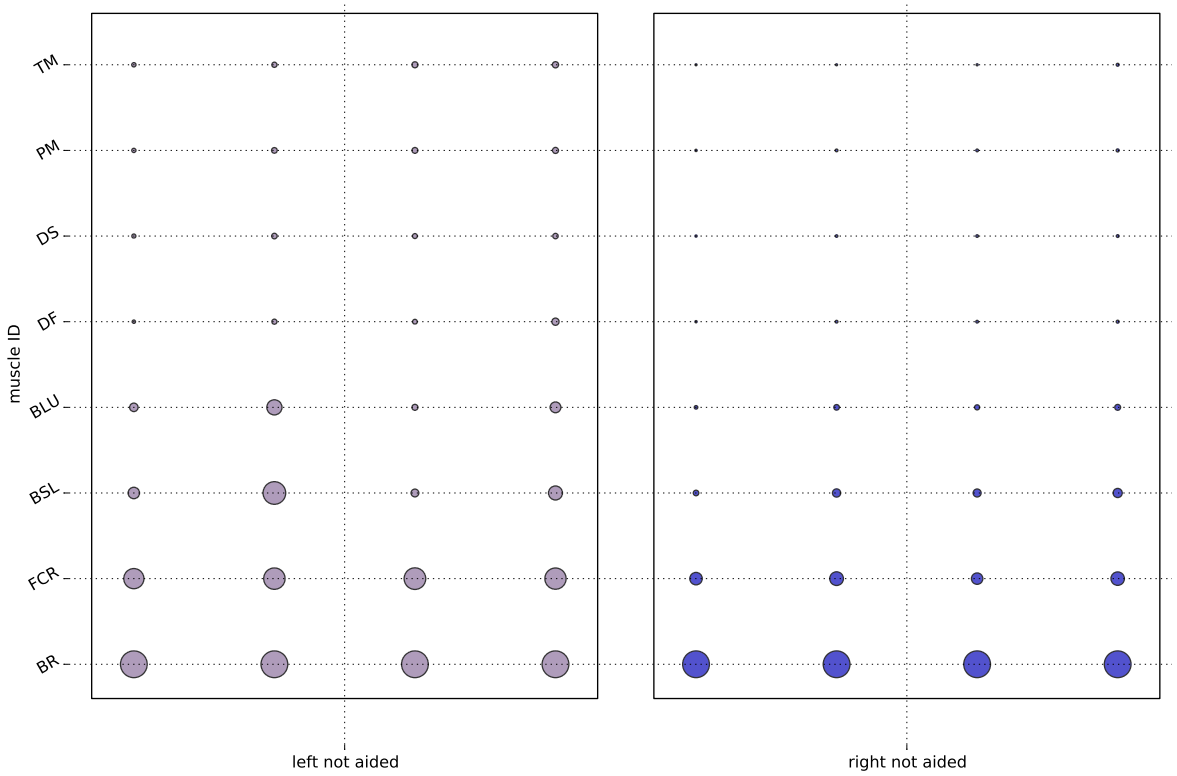


Fig. A.43: Muscle contribution summed for each synergy and calculated by NMF for every repetition during excercise `CF` of reference subject `R_R2`, legend see fig. 6

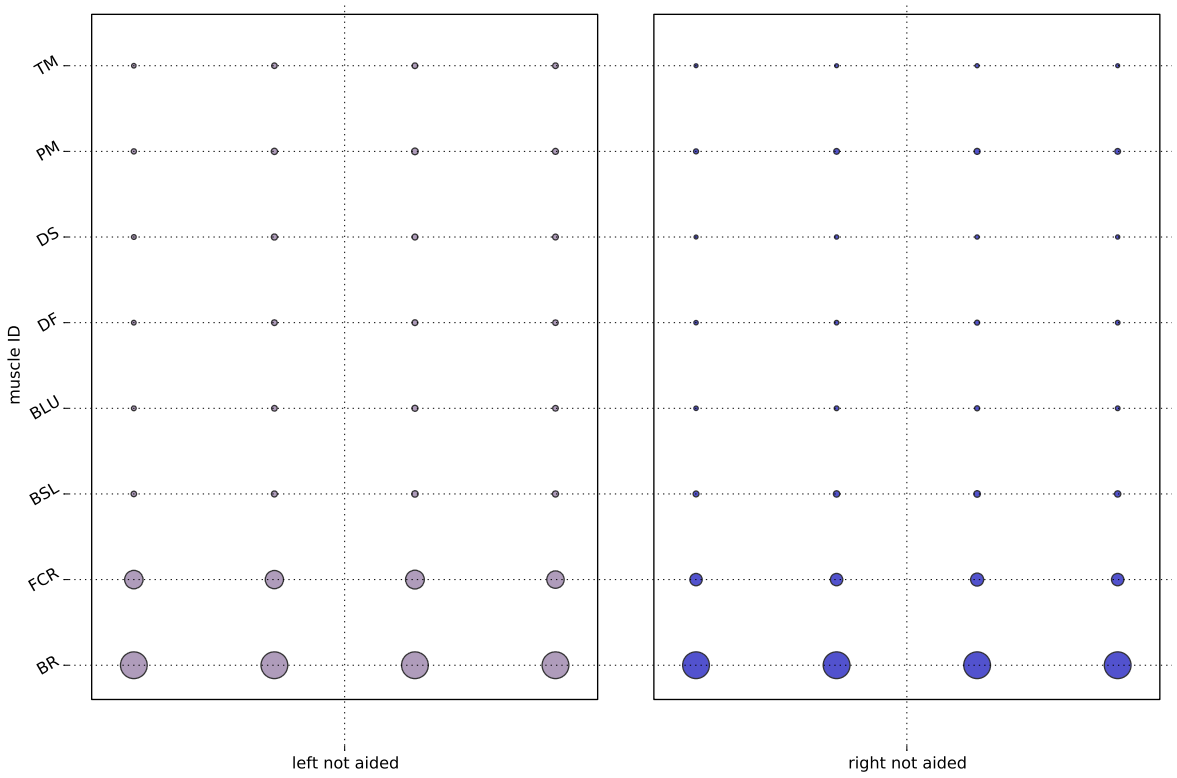


Fig. A.44: Muscle contribution summed for each synergy and calculated by NMF for every repetition during excercise CF of reference subject R_P1, legend see fig. 6

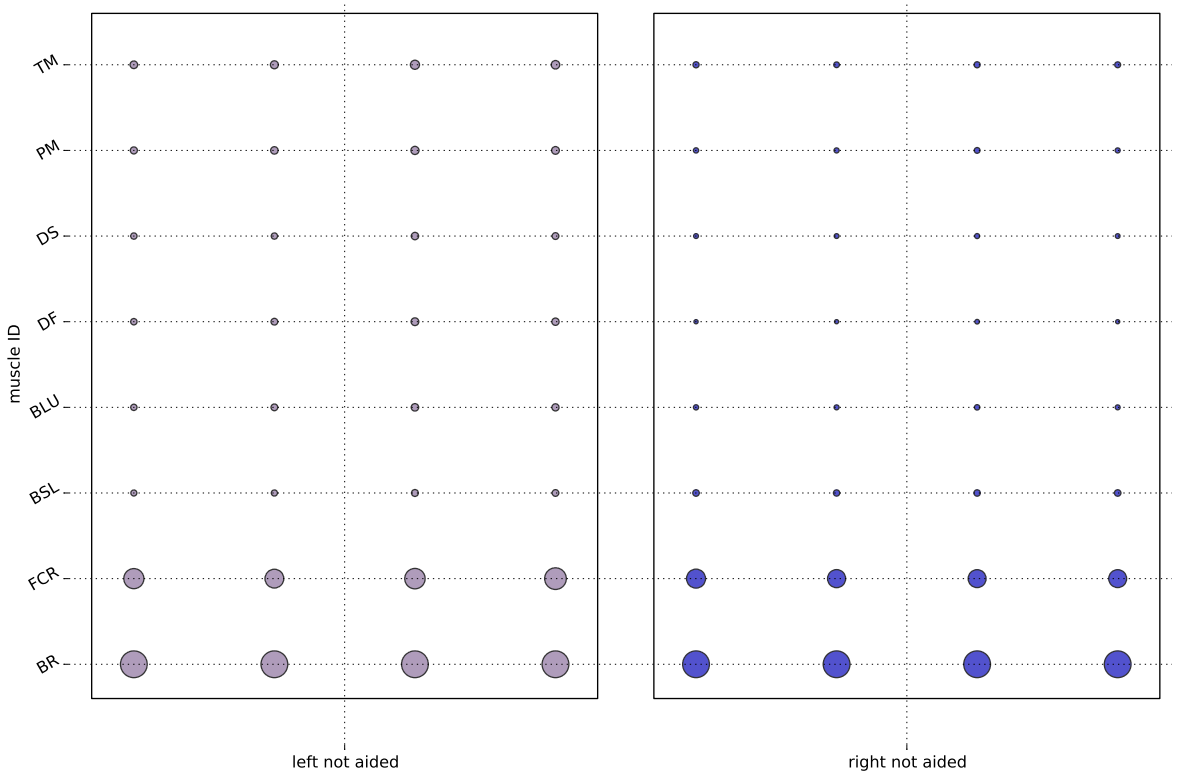


Fig. A.45: Muscle contribution summed for each synergy and calculated by NMF for every repetition during excercise CF of reference subject R_P2, legend see fig. 6

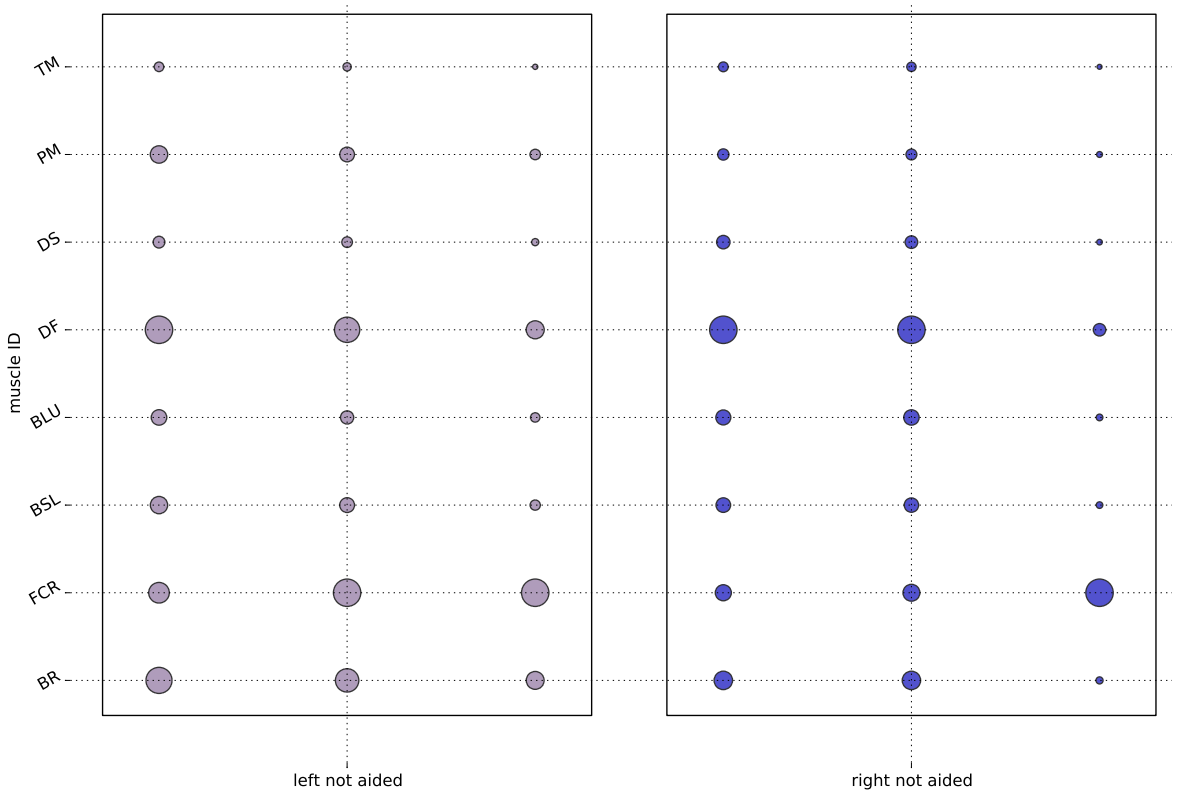


Fig. A.46: Muscle contribution summed for each synergy and calculated by NMF for every repetition during excercise CF of patient P_2, legend see fig. 6

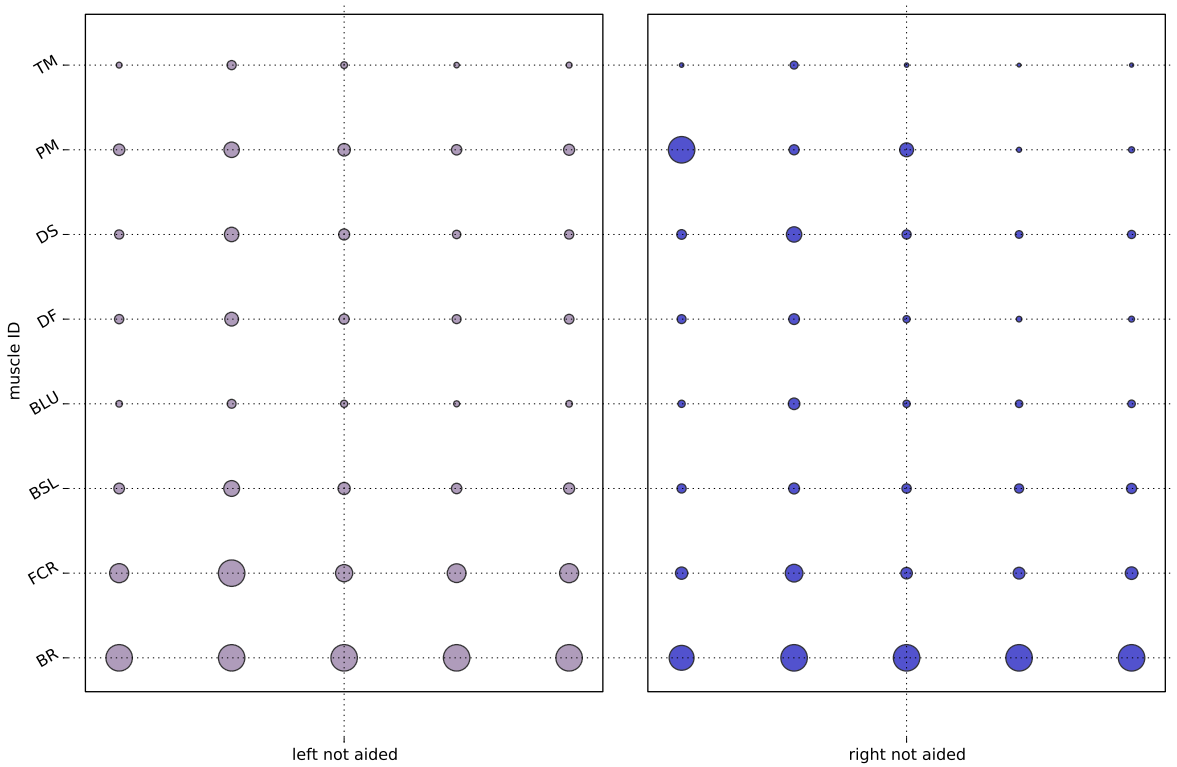


Fig. A.47: Muscle contribution summed for each synergy and calculated by NMF for every repetition during excercise CF of patient P_3, legend see fig. 6

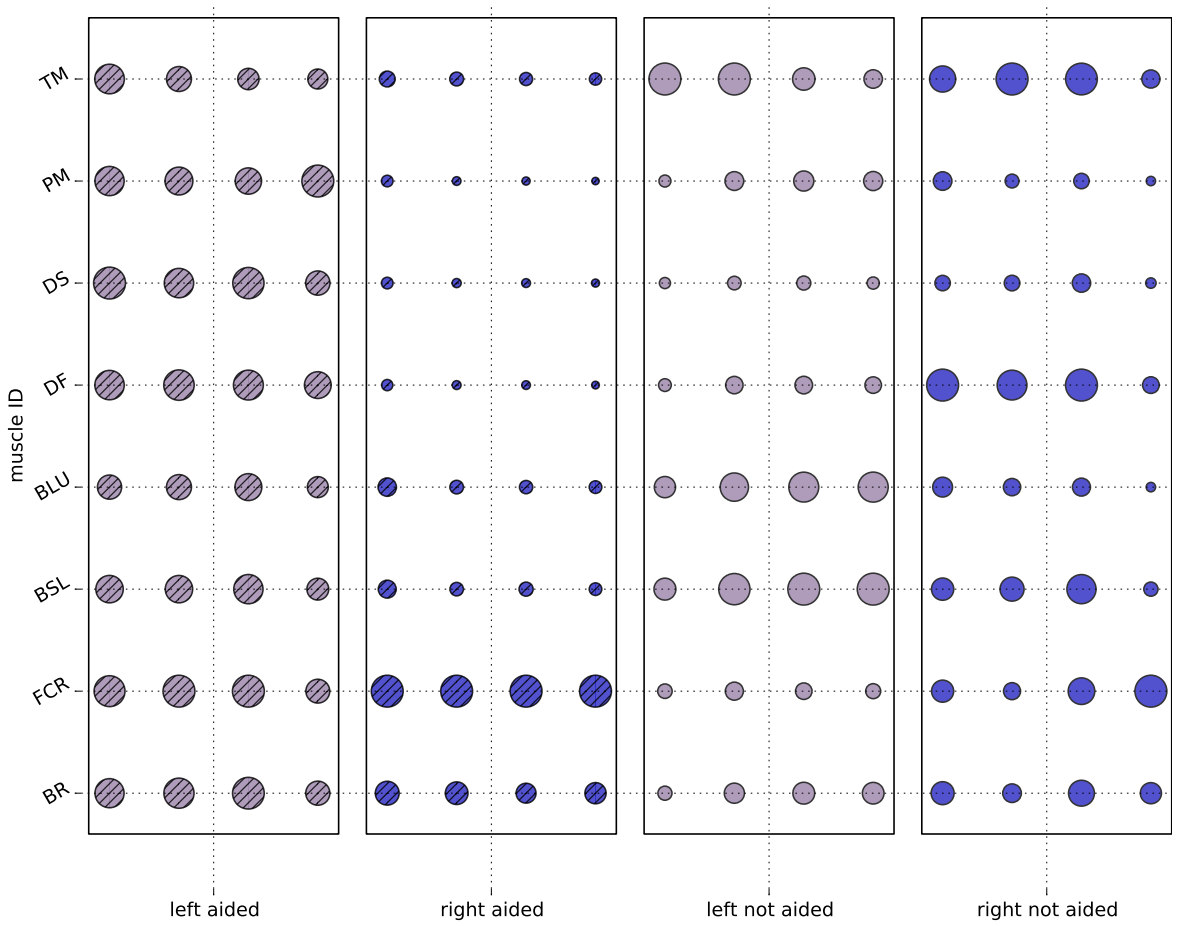


Fig. A.48: Muscle contribution summed for each synergy and calculated by NMF for every repetition during excercise CF of patient P_4, legend see fig. 6

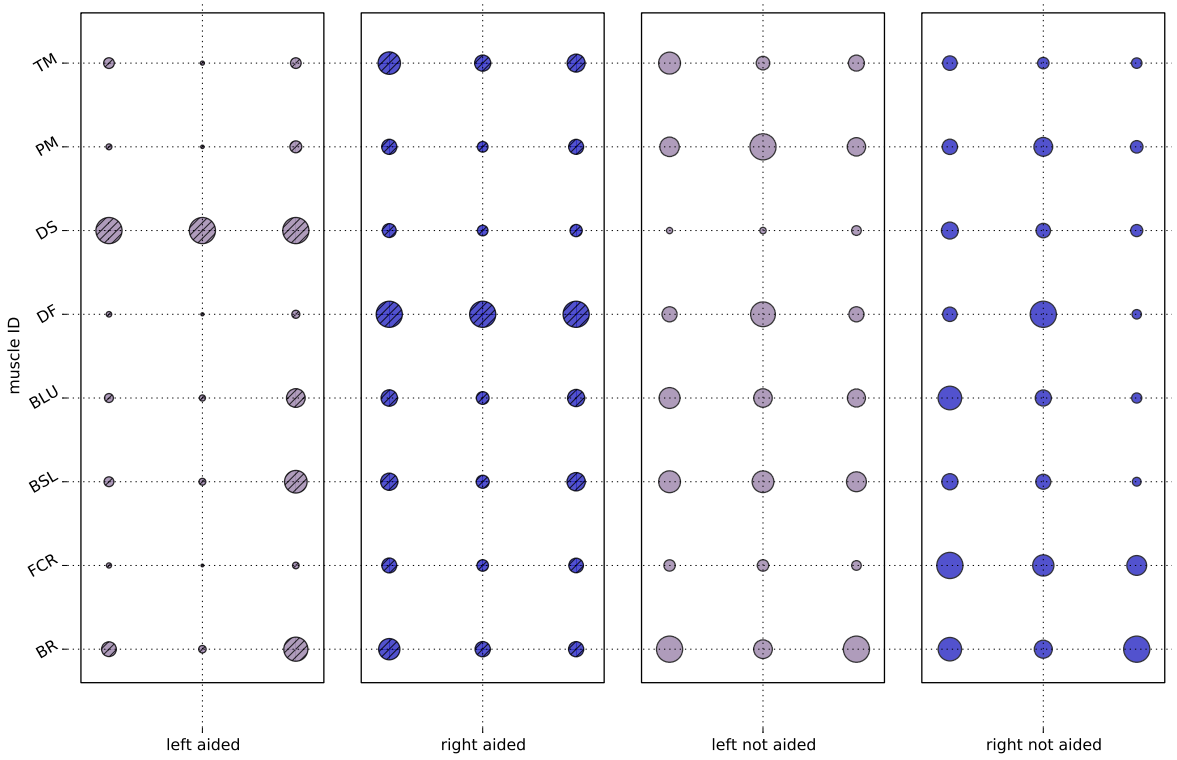


Fig. A.49: Muscle contribution summed for each synergy and calculated by NMF for every repetition during excercise CF of patient P_5, legend see fig. 6

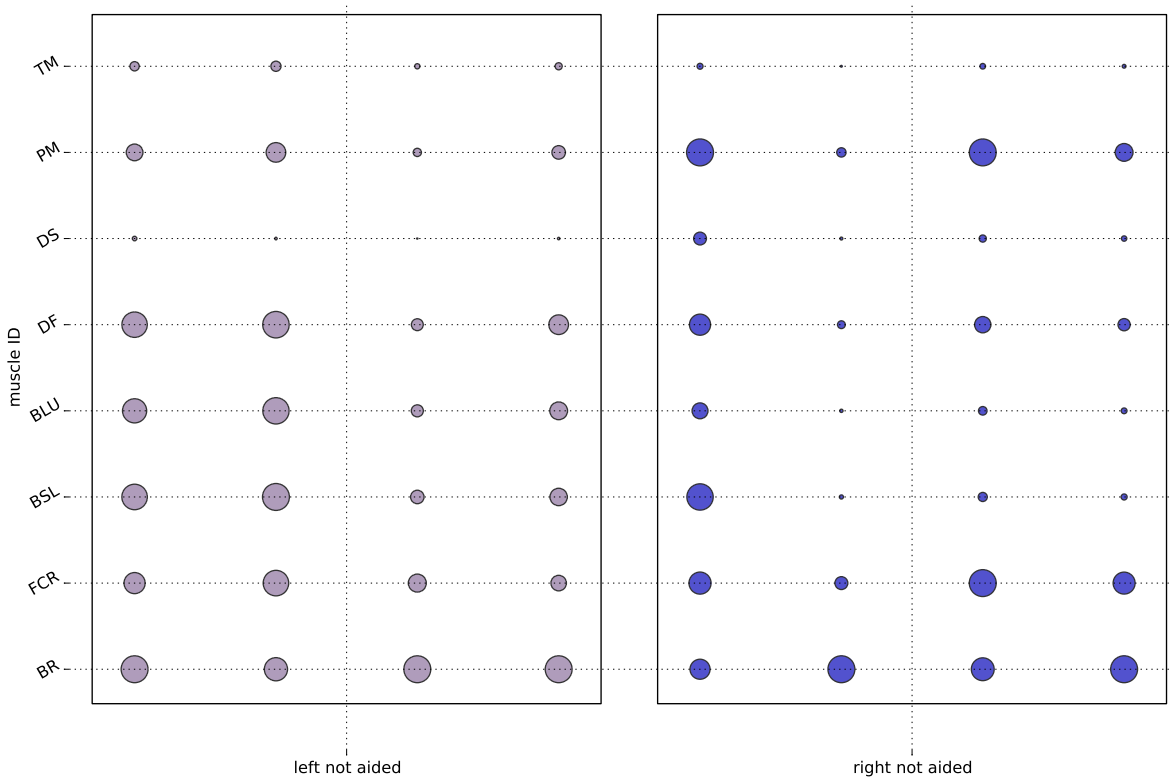


Fig. A.50: Muscle contribution summed for each synergy and calculated by NMF for every repetition during excercise CF of patient P_6, legend see fig. 6

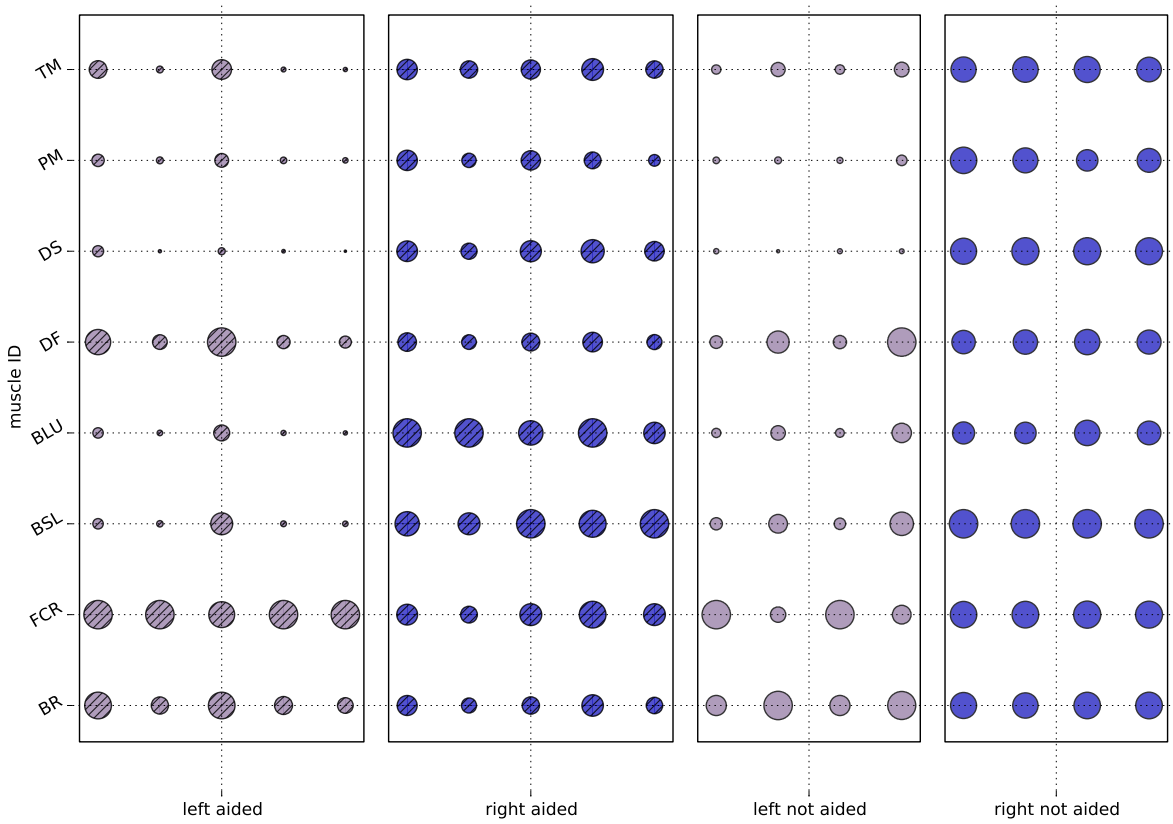


Fig. A.51: Muscle contribution summed for each synergy and calculated by NMF for every repetition during excercise CF of patient P_7, legend see fig. 6

## B. References


Artemiadis, Panagiotis K and Kyriakopoulos, Kostas J. Emg-based control of a robot arm using low-dimensional embeddings. *Robotics, IEEE Transactions on*, 26(2):393 – 398, 2010.

Becker, H. Identification and characterization of events in social media. PhD thesis, Columbia University, 2011.

Borgefors, Gunilla. Distance transformations in digital images. *Computer Vision, Graphics, and Image Processing*, 34(3):344 – 371, 1986.

Canny, John. A computational approach to edge detection. *Pattern Analysis and Machine Intelligence, IEEE Transactions on*, PAMI-8(6):679 – 698, Nov 1986. ISSN 0162-8828.

Cheung, Vincent CK, Piron, Lamberto, Agostini, Michela, Silvoni, Stefano, Turolla, Andrea, and Bizzi, Emilio. Stability of muscle synergies for voluntary actions after cortical stroke in humans. *Proceedings of the National Academy of Sciences*, 106 (46):19563 – 19568, 2009.

Coates, Adam and Ng, Andrew Y. Learning feature representations with k-means. In Montavon, Grégoire, Orr, Geneviève, and Müller, Klaus-Robert (eds.), *Neural Networks: Tricks of the Trade*, chapter 22. Springer, 2nd edition, 2012.

Corning, Peter A. The synergism hypothesis. *Journal of Social and Evolutionary Systems*, 21(2):133 – 172, 1998.

Delsys. Trigno wireless system. `http://www.delsys.com/Attachments_pdf/Trigno%20System%20(DOC-121-3-0).pdf`, January 2014.

Doerschuk, Peter C, Gustafon, Donald E, and Willsky, Alan S. Upper extremity limb function discrimination using emg signal analysis. *Biomedical Engineering, IEEE Transactions on*, BME-30(1):18 – 29, 1983. ISSN 0018-9294.

GNU. *GNU online documentation: atan2 - arctangent function*, 4.0.2 edition, February 2014. URL `http://gcc.gnu.org/onlinedocs/gcc-4.0.2/gfortran/ATAN2.html`.

Golub, Gene H. and Van Loan, Charles F. *Matrix computations (3rd ed.)*. Johns Hopkins University Press, 1996. ISBN 0801854148.

Gonzales, R and Woods, R. *Digital Image Processing*. Addison-Wesley Publishing Company, 1992.

Guillemard. On dimensional reduction techniquies in signal processing and apllications in emg analysis. Master's thesis, Universität Hamburg, June 2008.

Hartley, R. and Zisserman, A. *Multiple View Geometry in Computer Vision*. Cambridge books online. Cambridge University Press, 2003. ISBN 9781139449144.

Hussain, MS, Reaz, MBI, Ibrahimy, MI, Mastorakis, NE, Mladenov, V, Bojkovic, Z, Simian, D, Kartalopoulos, S, Varonides, A, Udriste, C, et al. Semg signal processing and analysis using wavelet transform and higher order statistics to characterize muscle force. In *WSEAS International Conference. Proceedings. Mathematics and Computers in Science and Engineering*, number 12. WSEAS, 2008.

Jean, J.S. *Kinect Hacks: Tips & Tools for Motion and Pattern Detection*. Hacks series. O'Reilly Media, 2012. ISBN 9781449361235.

Jiang, Ching-Fen, Lin, Yu-Ching, and Yu, Nan-Ying. Multi-scale surface electromyography modeling to identify changes in neuromuscular activation with myofascial pain. *Neural Systems and Rehabilitation Engineering, IEEE Transactions on*, 21(1):88 – 95, 2013.

Kullback, S. and Leibler, R. A. On information and sufficiency. *The Annals of Mathematical Statistics*, 22(1):79–86, 1951.

Li, Junning, Wang, Z Jane, Eng, Janice J, and McKeown, Martin J. Bayesian network modeling for discovering dependent synergies among muscles in reaching movements. *Biomedical Engineering, IEEE Transactions on*, 55(1):298 – 310, 2008.

Rafiee, J, Rafiee, MA, Yavari, F, and Schoen, MP. Feature extraction of forearm emg signals for prosthetics. *Expert Systems with Applications*, 38(4):4058 – 4067, 2011.

Reaz, M.B.I., Hussain, M.S., and Mohd-Yasin, F. Techniques of emg signal analysis: detection, processing, classification and applications. *Biological Procedures Online*, 8(1):11 – 35, 2006.

Reinkensmeyer, David J., Iobbi, Mario G., Kahn, Leonard E., Kamper, Derek G., and Takahashi, Craig D. Modeling reaching impairment after stroke using a population vector model of movement control that incorporates neural firing-rate variability. *Neural Computation*, 15(11):2619 – 2642, 2003.

Rosenberg, Andrew and Hirschberg, Julia. V-measure: A conditional entropy-based external cluster evaluation measure. In *Proceedings of the 2007 Joint Conference on Empirical Methods in Natural Language Processing and Computational Natural Language Learning (EMNLP-CoNLL)*, pp. 410 – 420, 2007.

Rousseeuw, Peter. Silhouettes: A graphical aid to the interpretation and validation of cluster analysis. *J. Comput. Appl. Math.*, 20(1):53 – 65, 1987. ISSN 0377-0427.

Salman, Berna. Changes in patterns of emg activity in post-stroke subjects following robot-assisted hand rehabilitation. Master's thesis, School of Kinesiology-Simon Fraser University, 2009.

Sandercock, P. Strokepathophysiology, diagnosis, and management, 4th edition. *Journal of Neurology, Neurosurgery & Psychiatry*, 76(1):148 – 149, 2005.

Soille, Pierre. *Morphological Image Analysis: Principles and Applications*. Springer-Verlag New York, Inc., 2 edition, 2003. ISBN 3540429883.

Ting, L.H. and Chvatal, S.A. *5 - Decomposing Muscle Activity in Motor Tasks: Methods and Interpretation*. Oxford University Press, USA, 2010. ISBN 9780199780785.

Vogel, J., Bayer, J., and van der Smagt, P. Continuous robot control using surface electromyography of atrophic muscles. In *Intelligent Robots and Systems (IROS), 2013 IEEE/RSJ International Conference on*, pp. 845–850, 2013.

Warlow, C.P., van Gijn, J., Dennis, M.S., Wardlaw, J.M., Bamford, J.M., Hankey, G.J., Sandercock, P.A.G., Rinkel, G., Langhorne, P., Sudlow, C., et al. *Stroke: Practical Management*. Wiley, 2008. ISBN 9780470695654.

Wiesendanger, Mario, Kaluzny, Pawel, Kazennikov, Oleg, and Perrig, Stephen. 14 - two hands - one action: The problem of bimanual coordination. In Wing, Alan M., Haggard, Patrick, and Flanagan, J. Randall (eds.), *Hand and Brain*, pp. 283 – 300. Academic Press, 1 edition, 1996. ISBN 978-0-12-759440-8.

Wolf, Steven L, Butler, Andrew J, Alberts, Jay L, and Kim, Min Wook. Contemporary linkages between emg, kinetics and stroke rehabilitation. *Journal of Electromyography and Kinesiology*, 15(3):229 – 239, 2005.

## C. Acronyms

| | |
|---|---|
| EMG | Electromyography. |
| GSK | Gain Shape k-Means. |
| NMF | Non-negative Matrix Factorization. |
| PCA | Principal Component Analysis. |
| RGBD | RGB+Depth. |
| RMS | Root Mean Square. |
| sEMG | Surface Electromyography. |

## D. List of Symbols

| | |
|---|---|
| $E$ | Number of electrodes. |
| $e$ | index of an electrode. |
| $L$ | reduced number of dimensions. |
| $\|v\|_0$ | l0-norm defined by number of non-zero entries of vector $v$. |
| $\mu_x$ | mean of signal $x$. |
| $\mu_x^e$ | mean of EMG signal $x^e$. |
| $N$ | Number of samples. |
| $N_w$ | windows size. |
| $\sigma_x^2$ | variance of signal $x$. |
| $\sigma_x^{e\,2}$ | variance of EMG signal $x^e$. |
| $W$ | basis matrix for dimensionality reduction and matrix decomposition. |
| $X$ | EMG input matrix with $E$ columns and $N$ rows. |
| $X[n]$ | $n$th row vector of matrix $X$. |
| $x^e$ | EMG signal vector of electrode $e$. |
| $x^e_{sub}$ | EMG signal vector $x$ of electrode $e$ with subset indicating the slection criterion. |
| $(X)_{i,k}$ | element of matrix $X$ at row $i$ and column $k$. |